

Manuscript Number: JSSC-19-979R1

Title: Synthesis and Optical Properties RE₂O₂S:Ln (RE = La, Y; Ln = Ce, Eu, Dy, Er)

Article Type: Research Paper

Keywords: oxysulfides, sulfates, rare-earth, reduction, optical ceramic, luminescence

Corresponding Author: Dr. Elena I Sal'nikova, Ph.D.

Corresponding Author's Institution: Northern Trans-Ural Agricultural University

First Author: Elena I Sal'nikova, Ph.D.

Order of Authors: Elena I Sal'nikova, Ph.D.; Yuriy G Denisenko; Alexander S Aleksandrovsky, Ph.D.; Ilya E Kolesnikov, Ph.D.; Erkki Lähderanta, Ph.D.; Petr O Andreev; Nikita O Azarapin, Ph.D.; Oleg V Andreev, Dr.; Sofia A Basova; Aleksei V Matigorov

Abstract: The phase formation sequence was studied in the preparation of solid solutions of RE₂O₂S: Ln' (RE = La, Y; Ln' = Ce, Eu, Dy, Er) by the reduction of the match co-precipitated sulfates, followed by sulfidization of the reduction products. For uniform distribution of cations in the matrix, a method of chemical homogenization was used, consisting in the preparation of an aqueous solution containing all the necessary cations and their subsequent precipitation in the form of sulphates. The use of sulfates as precursors facilitates the process of obtaining solid solutions of oxysulfides, since sulfates already contain SO₄²⁻ ions. The phase and morphological certification of the obtained solid solutions was carried out. The study of steady state luminescent properties demonstrated characteristic bands which are assigned to 4f-4f and 5d-4f transition. The obtained results showed the possibility of applying the method to synthesize optical ceramics based on solid solutions RE₂O₂S: Ln (RE = La, Y; Ln = Ce, Eu, Dy, Er).

Elena I. Sal'nikova
Institute of Chemistry

Dear Anthony Powell

Our team of authors is grateful for the submitted reviews.

All comments and suggestions have been taken into account, as far as possible, which is reflected in the "Responses to reviewers" and the corrected version of the manuscript.

We confirm that this study presents original research.

We have no conflict of interest in this work.

We look forward to a long and fruitful cooperation with your magazine.

E.I. Salnikova

17/09/2019

Response to Reviews

The authors are grateful to the editor and reviewers for their comments on our article. Sy tried to take them all into account and make the necessary adjustments to the article. Below are our answers.

Reviewer #1: The article titled "Synthesis and Optical Properties RE₂O₂S:Ln (RE = La, Y; Ln = Ce, Eu, Dy, Er)" describes the preparation of activated oxysulfides and their properties. Although the article is short, authors have discussed the synthesis and characterizations in detail. The following questions might be helpful:

-How did authors certify the phase compositions of each materials? Is there any elemental analysis performed?

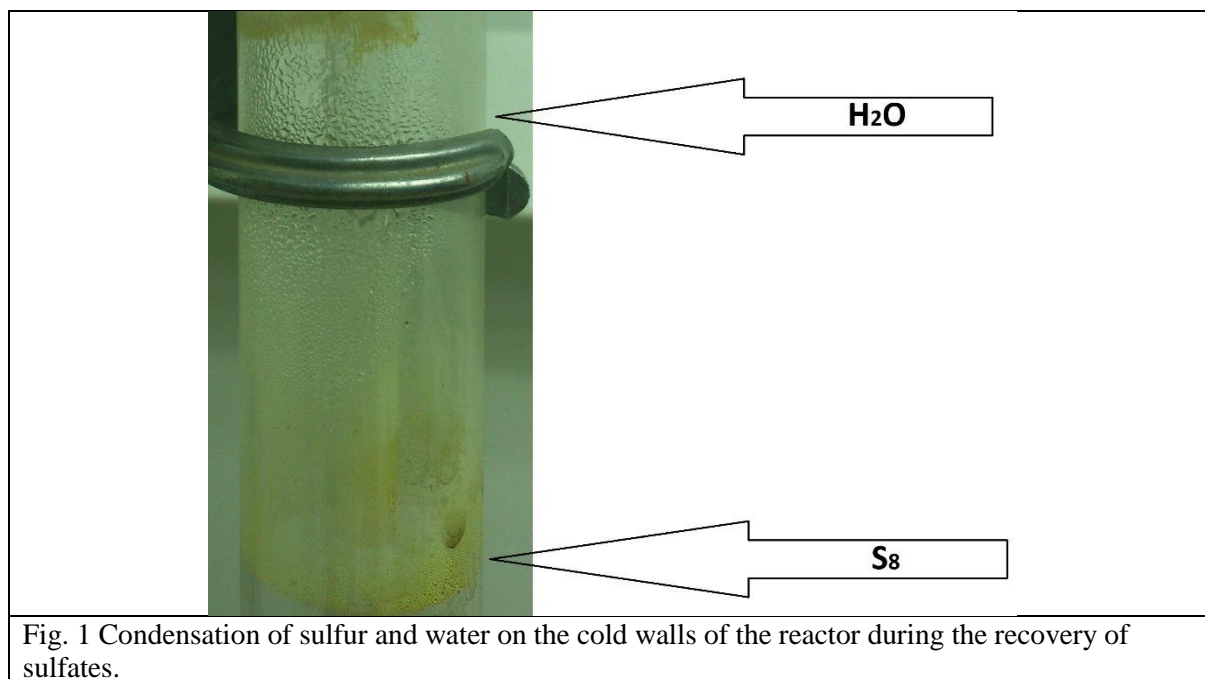
In this study, the phase composition was studied only by X-ray phase analysis, using the Rietveld method to process the results. The statistical processing parameters have good values for both multiphase and single-phase samples. Changing the parameters of an elementary cell completely correlates with the degree of doping, which confirms the formation of solid solutions, rather than two-phase samples.

-Thermogravimetric analysis/any other relevant experiment should be reported that supports the suggested reaction equations (e.g., page 5 line 35-38, etc.).

Unfortunately, we have no opportunity to conduct thermogravimetric analysis in a restorative atmosphere. The equations are based on the analysis of a large amount of experimental data. Solid reaction products are described based on x-ray phase analysis data. By-products are determined based on experimental observations in the synthesis process. Elemental sulfur and water are released at the very first stages of synthesis and condense on the cold walls of the reactor (Fig. 1). That allows you to uniquely identify them.

At certain stages of the synthesis at low temperatures, the off-gas does not give a reaction when sparging them through a solution of lead nitrate. However, when they are sparged through a barium nitrate solution, a white precipitate soluble in nitric acid precipitates. Based on this, it was concluded that at certain stages of the synthesis, a shallow reduction to sulfur dioxide can occur.

Unambiguous writing of the reaction equations is most likely impossible. All the written reaction equations are possible from the thermodynamic point of view and are most likely coupled during the process of sulfate reduction.



-Graphical abstract for this article is missing.

Graphical abstract corrected and submitted

-It would be better to have sub-sections under results and discussions to explain different observations.

The remark is taken into account in the manuscript of the article.

-The discussion on morphological transformation requires more explanation and details (page 6, line 4-8, fig 2).

Corresponding discussions and comparison with the literature data are presented in the text of the article.

The article needs to address the above-mentioned concerns/questions before it can be considered in JSSC.

Reviewer #2: Manuscript Number JSSC-19-979 reports on a synthesis method for lanthanide doped sulfide oxides and their optical properties. There are some minor issues to be resolved before it can be published.

- abstract: There are no S^{6+} cations in sulphates. Oxidation state and charge is not the same!

Corrected

- introduction: "thermal destruction method" is an unusual term. Maybe call it "thermal decomposition" or "combustion"?

Replaced by the term "Thermal decomposition"

- results and discussion: For the syntheses the formation of either S or SO₂ was proposed. Please explain, how this was proven.

Unfortunately, we have no opportunity to conduct thermogravimetric analysis in a restorative atmosphere. The equations are based on the analysis of a large amount of experimental data. Solid reaction products are described based on x-ray phase analysis data. By-products are determined based on experimental observations in the synthesis process. Elemental sulfur and water are released at the very first stages of synthesis and condense on the cold walls of the reactor (Fig. 1). That allows you to uniquely identify them.

- space group symbols: Please write space group symbols according to the common style as seen e. g. in the International Tables for Crystallography throughout text and tables.

Corrected

- figure 1 caption: The figure does not only show difference, but also observed and calculated patterns.

Corrected

Reviewer #3: In this manuscript the authors present a method for the production of luminescent materials on the basis of rare earth oxysulfides. The results presented are interesting and the conclusions are adequately supported by the results and discussions presented. After the revisions made by the authors the manuscript is almost ready for publication, I suggest some minor corrections:

The authors should standardize throughout the text "rare-earth" or "rare earth"

Page 1, line 46 the authors should be put a space between "used" and "in"

Page 2, lines 16 and 17 the authors should be replaced "mol/l" to "mol/L"

Page 2, lines 21,22,23 and 27 the authors should be replaced "ml" to "mL"

All comments are taken into account and adjustments are made to the article.

1 Corresponding author: E.I. Sal'nikova
2 Tyumen State University, Tyumen 625003, Russia
3 E-mail: elenasalnikova213@gmail.com
4

5 **Synthesis and Optical Properties RE₂O₂S:Ln (RE = La, Y; Ln = Ce, Eu, Dy, Er)**

6
7 E.I. Sal'nikova^{1,2}, Yu.G. Denisenko³, A.S. Aleksandrovsky^{4,5}, I.E. Kolesnikov^{6,7}, E. Lähderanta⁷,
8 P.O. Andreev¹, N.O. Azarapin¹, O.V. Andreev¹, S.A. Basova¹, A.V. Matigorov¹
9

10 ¹Department of Inorganic and Physical Chemistry, Tyumen State University, Tyumen 625003, Russia

11 ²Department of General Chemistry, Northern Trans-Ural Agricultural University, Tyumen, 625003, Russia

12 ³Department of General and Special Chemistry, Industrial University of Tyumen, Tyumen 625000, Russia

13 ⁴Laboratory of Coherent Optics, Kirensky Institute of Physics Federal Research Center KSC SB RAS,
14 Krasnoyarsk 660036, Russia

15 ⁵Institute of Nanotechnology, Spectroscopy and Quantum Chemistry, Siberian Federal University,
16 Krasnoyarsk 660041, Russia

17 ⁶Center for Optical and Laser Materials Research, St. Petersburg State University, St. Petersburg 199034,
18 Russia

19 ⁷Department of Physics, Lappeenranta University of Technology LUT, Lappeenranta 53850, Finland
20
21

22 **Abstract**

23 The phase formation sequence was studied in the preparation of solid solutions of RE₂O₂S: Ln' (RE = La, Y;
24 Ln' = Ce, Eu, Dy, Er) by the reduction of the match co-precipitated sulfates, followed by sulfidization of the
25 reduction products. For uniform distribution of cations in the matrix, a method of chemical homogenization
26 was used, consisting in the preparation of an aqueous solution containing all the necessary cations and their
27 subsequent precipitation in the form of sulfates. The use of sulfates as precursors facilitates the process of
28 obtaining solid solutions of oxysulfides, since sulfates already contain SO₄²⁻-ions. The phase and
29 morphological certification of the obtained solid solutions was carried out. The study of steady state
30 luminescent properties demonstrated characteristic bands which are assigned to 4*f*-4*f* and 5*d*-4*f* transition.
31 The obtained results showed the possibility of applying the method to synthesize optical ceramics based on
32 solid solutions RE₂O₂S: Ln (RE = La, Y; Ln = Ce, Eu, Dy, Er).
33
34

35 **Keywords:** oxysulfides, sulfates, rare-earth, reduction, optical ceramic, luminescence
36

37 **1. Introduction**

38 Oxygen-containing compounds of rare-earth elements have long attracted the attention of researchers
39 due to their effective luminescent properties, which have found application in many optical systems [1-
40 6]. Despite the fact that the luminescence is mainly determined by the nature of the substituting ion, the host
41 matrix into which this ion is embedded influences on the emission lines intensity through its crystal field [7-
42 10]. Lanthanide ions can emit light in the near UV, visible and infrared regions of the spectrum. Each ion
43 has a characteristic absorption and emission spectrum. Ln³⁺ radiation is characterized by high color purity;
44 therefore, materials activated by lanthanides are attractive for creating LEDs, fluorescent lamps, plasma
45 displays, and active media for solid-state lasers [11-13].

46 Activated materials based on oxysulfides of rare-earth elements are widely used in various fields [14-
47 22]. However, in recent years, only laborious, poorly reproducible methods of producing nanoparticles are

described in the literature for these objects. At the same time, the need for relatively simple synthesis methods allowing large batches of optical ceramics does not decrease[23–27].

Thermal decomposition methods are convenient for obtaining materials with different properties [28–32]. In the preparation of oxysulfides, particular attention is drawn to methods for reducing sulfur containing compounds to higher oxidation degrees. Compared with solid-phase methods, the recovery method differs in manufacturability, reproducibility, and the ability to produce several tens of grams of a product at once [33–39].

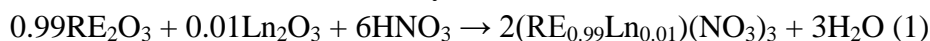
Thus, the aim of the work is to study the chemistry of reactions in the sequential processing of co-precipitated sulfates of rare earth elements in the atmosphere of H₂, H₂S to obtain activated oxysulfides and investigate the morphology of the obtained reaction products and their luminescent properties.

2. Materials and methods

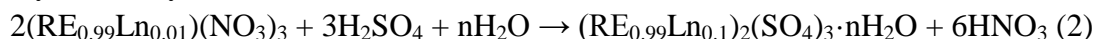
2a. Preparative Methods

Powders of co-precipitated sulfates were obtained by precipitation from a nitrate solution with concentrated sulfuric acid. For the synthesis, high purity reagents were used: Ln₂O₃ (≥99.99%, ultrapure, TDM-96 Ltd. Russia). Concentrated nitric acid solution (C(HNO₃) = 14.6 mol/L, ultrapure, Vekton Ltd., Russia), concentrated sulfuric acid solution (C (H₂SO₄) = 17.9 mol/L, ultrapure, Vekton Ltd., Russia). Weighing was carried out on an analytical balance with an accuracy of 0.1 mg. Before weighing, the oxides were calcined in a muffle furnace at a temperature of 1000°C for 12 hours to remove sorbed gases and products of their interaction with oxides (Ln(OH)₃, Ln₂(CO₃)₂). Acid solutions were measured using glass measuring cylinders with an accuracy of 0.1 ml.

The calculated weighed amount of oxides with a total weight of 5.0 g was placed in a 100 mL glass round-bottom flask, then 7.0 mL of a concentrated solution of nitric acid was poured in small portions. The reaction mixture was heated on a mantle until the oxides were completely dissolved. As a result, a nitrate solution was obtained with evenly distributed cations:



After cooling the solution, 3.0 ml of concentrated sulfuric acid was poured in small portions to it, avoiding strong heating of the reaction mixture. As a result, a precipitate of co-precipitated sulfates and their crystalline hydrates forms:



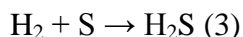
After carrying out the precipitation reaction, the reaction mixture is distilled off to the dry residue. The obtained polycrystalline product is additionally calcined in a tubular furnace at a temperature of 500°C to remove sorbed moisture and acids. Later, the powder is annealed at the same temperature for 7 days, in order to form an acceptable crystallite structure.

This method of chemical homogenization has a number of significant advantages:

- In the process of synthesis, no cations other than Ln³⁺ are added to the reaction mixture, which excludes their replacement and the formation of defects in the crystal structure.
- Sulfates precipitate from a homogeneous nitrate solution, which ensures high stoichiometry and uniform distribution of cations within the crystal lattice.
- Conducting the reaction in an environment of concentrated sulfuric acid allows to form the structure of anhydrous sulfate at the earliest stages.

The reduction of sulfates in a hydrogen atmosphere was carried out on the apparatus shown in Figure S1. High purity hydrogen was obtained by the electrolytic method in the SPECTR - 6M hydrogen generator. The temperature in the furnace was set using a microprocessor controller. The temperature in the furnace was controlled using chromel-alumel thermocouple. A weighed amount of co-precipitated sulfates was placed in a quartz reactor, and for 30 minutes it was purged with hydrogen from a generator at a rate of 6

1 L/h. After that, the reactor was placed in a heated vertical furnace and kept for the required amount of time.
2 After completion of the process, the reactor was removed from the furnace and cooled to room temperature.
3 Processing of the reduced products in an atmosphere of hydrogen sulfide was carried out on a similar setup
4 (Fig. S2). The difference lies in the fact that before being fed into the reactor, the hydrogen passes through a
5 flask with molten elemental sulfur and heated to 350 °C. As a result, hydrogen sulfide is formed:



7 Consequently, it is not a hydrogen inflows the reactor, but a hydrogen sulfide.

9 **2b. Methods of physical-chemical analysis**

10 X-ray phase analysis (XRD) was performed on a BRUKER D2 PHASER diffractometer with a linear
11 detector LYNXEYE (CuK α radiation, Ni-filter). Rietveld refinement of all six samples was performed by
12 using TOPAS 4.2 [40]. Almost all peaks were indexed.

13 Electron-microscopic analysis was carried out on electron microscope JEOL JSM-6510LV. X-ray energy-
14 dispersive analyzer was used to register X-rays at element spectrum plotting in selected sample surface
15 areas. The inaccuracy in element content determination was equal to $\pm 0.2\%$.

16 All measurements of the luminescent properties were carried out on a research-grade spectrofluorimeter.
17 Horiba JobinYvon Fluorolog-3 equipped with double monochromators for excitation and emission channels
18 and 450 W xenon lamp as an excitation source.

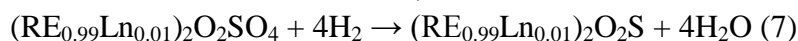
20 **3. Result and Discussion**

22 **3a. Synthetic experiment**

23 Detailed consideration of the chemical transformations taking place during the transformation of co-
24 precipitated sulfates into the corresponding solid solutions of oxysulfides was made on the basis of two
25 model systems $\text{La}_2(\text{SO}_4)_3:\text{Dy}^{3+}$ and $\text{Y}_2(\text{SO}_4)_3:\text{Er}^{3+}$. The results obtained were used to synthesize all other
26 solid solutions, which are reported in this work.

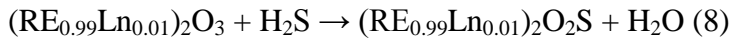
27 The carrying out of the co-precipitation of sulfates and the subsequent annealing led to the formation of
28 structures of solid solutions of sulfates in which the doping ion is fully incorporated into the crystal lattice of
29 the matrix and occupies the crystallographic positions of the host cation. According to X-ray diffraction
30 data, all samples of co-precipitated sulfates are single-phase (Fig. 1a, b). There is a slight shift in the unit
31 cell parameters caused by the difference in the radii of the cations of the matrix and the dopant.

32 The appearance of gaseous reduction products was recorded at a temperature of 570°C. In this connection,
33 sulfate reduction was carried out at $t = 600^\circ\text{C}$. At this temperature, after 60 minutes of the process, the
34 products mainly consist of 4 phases: $(\text{RE}_{0.99}\text{Ln}_{0.01})_2(\text{SO}_4)_3$ - $(\text{RE}_{0.99}\text{Ln}_{0.01})_2\text{O}_2\text{SO}_4$ - $(\text{RE}_{0.99}\text{Ln}_{0.01})_2\text{O}_2\text{S}$ -
35 $(\text{RE}_{0.99}\text{Ln}_{0.01})_2\text{O}_3$ (Fig. 1c, d). There was an incomplete transformation of the initial sulfates into the reaction
36 products. The following chemical equations correspond to the formation of the corresponding reduction
37 products:



42 After 10 hours of carrying out the process at a given temperature, polycrystalline products consist of two
43 phases: $(\text{RE}_{0.99}\text{Ln}_{0.01})_2\text{O}_2\text{S}$, $(\text{RE}_{0.99}\text{Ln}_{0.01})_2\text{O}_3$ (Fig. 1 e, f). The absence of compounds containing sulfur in the
44 highest degree of oxidation of in the synthesis products indicates on a complete redox transformation. In all
45 samples, the phase output $(\text{RE}_{0.99}\text{Ln}_{0.01})_2\text{O}_2\text{S}$ was not lower than 80%. Thus, the stage of sulfate reduction in
46 a hydrogen atmosphere allows the formation of two-phase polycrystalline intermediates with a predominant
47 content of the oxysulfide phase, which should greatly facilitate the sulfidation procedure.

1 The interaction of two-phase intermediates with hydrogen sulfide at a temperature of 800 ° C for 5 hours
2 leads to the formation of single-phase powders (RE_{0.99}Ln_{0.01})₂O₂S (Fig. 1 g, h). The transformation
3 corresponds to the transformation of the oxide phase to the oxysulfide under the action of a mild sulfiding
4 agent H₂S:



5 Sulfate powders, formed predominantly by loose agglomerates (Fig. 2, a) with sizes up to 10 μm. The
6 resulting oxysulfide powders have a more distinct cut shape, a denser structure and a uniform size
7 distribution (Fig. 2, a). The morphological transformation is evidently due to the elevated temperatures and
8 the diffusion character of the reduction and sulfidation processes.

9 The enlargement obviously occurs as a result of the desire of the system to lower its energy. What
10 corresponds to a decrease in the surface area of the polycrystalline samples. Particle cutting appears as a
11 result of high rates of chemical reactions and rapid mass transfer. The indicated tendency to particle
12 aggregation is often observed during similar processes [27, 32-35].

13 **3b. Structural and spectroscopic properties**

14
15 Crystal structure of both hosts belongs to *P-3m 1* space group of trigonal symmetry class. Y and La occupy a
16 single inequivalent site. In both oxysulfides the local environment of them is a distorted polyhedron with
17 seven vertices, four of them being oxygen ions and three being sulfur ions. Layered structure of oxysulfides
18 implies that sulfur and oxygen are positioned in opposite hemispheres of the local environment of either Y
19 or La. Rare-earth doping ions are expected to occupy Y and La sites, and their local environment is
20 determined by the structure host, with the local symmetry C_{3v}. Therefore, absence of inversion symmetry
21 must be pronounced in optical spectra of doping ions. Variation of luminescence properties of doping RE
22 ions in one host with respect to another is usually ascribed to the change of the extent of inversion symmetry
23 violation. Examining the geometry of local environment of RE ion in Y₂O₂S and La₂O₂S (Fig. 3) we observe
24 that both environments are geometrically identical.

25
26 The excitation and emission spectra of RE₂O₂S (RE = Y, La) activated by 1% of Dy³⁺ ions are shown in
27 Fig. 4. The observed spectra exhibit characteristic intra-configurational 4f-4f transitions. Excitation
28 spectrum of Y₂O₂S:Dy³⁺ monitored at 579 nm (⁴F_{9/2}-⁶H_{13/2}), displays following transitions: ⁶H_{15/2}-⁴P_{7/2} (355
29 nm), ⁶H_{15/2}-⁴P_{5/2} (369 nm), ⁶H_{15/2}-⁴I_{13/2} (388 nm), ⁶H_{15/2}-⁴G_{11/2} (427 nm), ⁶H_{15/2}-⁴I_{15/2} (451 nm) and ⁶H_{15/2}-
30 ⁴F_{9/2} (479 nm). The emission spectrum Y₂O₂S:Dy³⁺ sample is dominated by green-yellow band (579 nm)
31 corresponding to the hypersensitive ⁴F_{9/2}-⁶H_{13/2} transition. Other observed lines are attributed to the ⁴I_{15/2}-
32 ⁶H_{15/2} (457 nm), ⁴F_{9/2}-⁶H_{15/2} (487 nm), and ⁴F_{9/2}-⁶H_{11/2} (670 nm) transitions. It is well-known that ⁴F_{9/2}-⁶H_{13/2}
33 is the forced electric dipole transition, which is hypersensitive and its intensity can vary by orders of
34 magnitude depending on the local site symmetry, whereas ⁴F_{9/2}-⁶H_{15/2} transition intensity is insignificantly
35 affected by the environment [40-42]. The excitation and emission spectra of La₂O₂S:Dy³⁺ are similar to the
36 Y₂O₂S:Dy³⁺ ones. Small blue shift of bands and redistribution between them were observed. So, the most
37 prominent transitions in excitation and emission spectra of La₂O₂S:Dy³⁺ are centered at 353 and 576 nm,
38 respectively. Observed luminescence spectra of Dy ion are consistent with the concept that they occupy
39 Y(La) sites with the local symmetry C_{3v}.

40 To compare the crystal structure and crystal field of Y₂O₂S:Dy³⁺ and La₂O₂S:Dy³⁺ powders, we calculated
41 ratio (*R*_{Dy}) between ⁴F_{9/2}-⁶H_{13/2} and ⁴F_{9/2}-⁶H_{15/2} intensities. This parameter is similar to the well-known
42 asymmetry ratio for Eu³⁺ ions [43, 44]. *R*_{Dy} value give information about the local surrounding and
43 environmental changes near the Dy³⁺ ions. The higher the calculated parameter is, the more apart from a
44 centrosymmetric geometry luminescent center is located. It is well-known that if Dy³⁺ is located at low
45 symmetry without the inversion symmetry, the yellow emission is the most intense of all the transitions, as
46 is the case with our synthesized nanocrystalline phosphors [45]. Experimental *R*_{Dy} values for Y₂O₂S:Dy³⁺

1 and $\text{La}_2\text{O}_2\text{S}:\text{Dy}^{3+}$ samples are 3.13 and 4.65. In view of geometrical identity of local environments, this
2 difference must be ascribed to the interplay between ionic radii of Y and La and the unit cell parameters, i.e.
3 closer ligands at the same degree of inversion symmetry violation.

4 The steady state luminescence spectra of $\text{RE}_2\text{O}_2\text{S}$ (RE = Y, La) powders doped with 1% of Er^{3+} ions are
5 presented in Fig. 5. The excitation spectrum of $\text{Y}_2\text{O}_2\text{S}:\text{Er}^{3+}$ was monitored at 549 nm ($^4\text{F}_{9/2}-^4\text{I}_{15/2}$) within
6 spectral range of 330–530 nm. It consists of $^4\text{I}_{15/2}-^4\text{G}_{7/2}$ (360 nm), $^4\text{I}_{15/2}-^4\text{G}_{9/2}$ (367 nm), $^4\text{I}_{15/2}-^4\text{G}_{11/2}$ (379
7 nm), $^4\text{I}_{15/2}-^2\text{H}_{9/2}$ (408 nm), $^4\text{I}_{15/2}-^4\text{F}_{3/2}$ (446 nm), $^4\text{I}_{15/2}-^4\text{F}_{5/2}$ (453 nm), $^4\text{I}_{15/2}-^4\text{F}_{7/2}$ (491 nm), and $^4\text{I}_{15/2}-^2\text{H}_{11/2}$
8 (522 nm). The emission spectrum includes narrow bands, which are assigned to the following transitions:
9 $^2\text{H}_{9/2}-^4\text{I}_{15/2}$ (409 nm), $^2\text{H}_{11/2}-^4\text{I}_{15/2}$ (524 nm), $^4\text{S}_{3/2}-^4\text{I}_{15/2}$ (549 nm), and $^4\text{F}_{9/2}-^4\text{I}_{15/2}$ (670 nm). The spectral line
10 positions of $\text{La}_2\text{O}_2\text{S}:\text{Er}^{3+}$ spectra are the same. Change of host leads to the intensity redistribution, which is
11 most pronounced for $^4\text{I}_{15/2}-^4\text{G}_{11/2}$ transition in the excitation spectrum.

12 Fig. 6 displays excitation and emission spectra of $\text{RE}_2\text{O}_2\text{S}$ (RE = Y, La) activated by 1% of Eu^{3+} ions. The
13 excitation spectrum of $\text{Y}_2\text{O}_2\text{S}:\text{Eu}^{3+}$ monitored at 545 nm ($^5\text{D}_1-^7\text{F}_1$) consists of following transitions: $^7\text{F}_0-^5\text{D}_4$
14 (353 nm), $^7\text{F}_0-^5\text{L}_7$ (378 nm) and $^7\text{F}_2-^5\text{D}_2$ (488 nm). The emission spectrum shows narrow bands originating
15 from $^5\text{D}_1$ and $^5\text{D}_0$ excited levels. Surprisingly, that the emission spectrum of $\text{Y}_2\text{O}_2\text{S}:\text{Eu}^{3+}$ is dominated by
16 transition $^5\text{D}_1-^7\text{F}_1$ (545 nm), whereas the most prominent luminescence bands are usually attributed to the
17 $^5\text{D}_0-^7\text{F}_j$ transition [46–48]. Such behavior was previously reported for $\text{La}_2\text{O}_2\text{S}:\text{Eu}^{3+}$ bulk phosphors [49, 50].
18 Dominance of $^5\text{D}_1$ emission can be explained by small phonon energy in regarded host, because significant
19 amount of ions relax to $^5\text{D}_1$ level after the UV excitation, and they radiatively decay to the ground state
20 before nonradiative decay to $^5\text{D}_0$ metastable level. We also observed $^5\text{D}_2-^7\text{F}_2$ (490 nm), $^5\text{D}_1-^7\text{F}_3$ (587 nm),
21 $^5\text{D}_0-^7\text{F}_1$ (592 nm), $^5\text{D}_0-^7\text{F}_2$ (621 nm) and $^5\text{D}_0-^7\text{F}_3$ (670 nm) transitions.

22 The excitation and emission spectra of $\text{La}_2\text{O}_2\text{S}:\text{Eu}^{3+}$ display situation, which is more usual for Eu^{3+} -doped
23 compounds. The excitation spectrum of $\text{Y}_2\text{O}_2\text{S}:\text{Eu}^{3+}$ monitored at 623 nm ($^5\text{D}_0-^7\text{F}_2$) consists of broad
24 intense band corresponding to charge transfer $\text{S}^{2-}-\text{Eu}^{3+}$ (338 nm) and low-intense line assigned to the typical
25 intra-configurational transitions of the Eu^{3+} ion: $^7\text{F}_0-^5\text{L}_6$ (394 nm), $^7\text{F}_0-^5\text{D}_2$ (466 nm), $^7\text{F}_0-^5\text{D}_1$ (536 nm) and
26 $^7\text{F}_1-^5\text{D}_0$ (593 nm). The emission spectrum is dominated by the forced electric dipole transition $^5\text{D}_0-^7\text{F}_2$ with
27 maximum at 623 nm. Other observed lines are attributed to the $^5\text{D}_1-^7\text{F}_1$ (538 nm), $^5\text{D}_1-^7\text{F}_2$ (555 nm), $^5\text{D}_1-^7\text{F}_3$
28 (586 nm), $^5\text{D}_0-^7\text{F}_1$ (594 nm), $^5\text{D}_0-^7\text{F}_3$ (670 nm) and $^5\text{D}_0-^7\text{F}_4$ (704 nm).

29 Due to the unique luminescence properties of Eu^{3+} ions, it is quite easy to analyze the luminescent center
30 local surrounding and its symmetry using only emission spectrum. The asymmetry ratio (R_{Eu}) gives
31 information about local changes around the Eu^{3+} ions. It is defined as intensity ratio of forced electric dipole
32 $^5\text{D}_0-^7\text{F}_2$ and magnetic dipole $^5\text{D}_0-^7\text{F}_1$ transitions. The higher the asymmetry parameter R_{Eu} is, the more apart
33 from a centrosymmetric geometry luminescent center is located. The calculated R_{Eu} values of $\text{Y}_2\text{O}_2\text{S}:\text{Eu}^{3+}$
34 and $\text{La}_2\text{O}_2\text{S}:\text{Eu}^{3+}$ samples are 0.58 and 3.16, respectively. It is worth noting that the calculated R_{Eu} values of
35 $\text{Y}_2\text{O}_2\text{S}:\text{Eu}^{3+}$ and $\text{La}_2\text{O}_2\text{S}:\text{Eu}^{3+}$ samples significantly differ, which indicate big difference in local surrounding
36 of Eu^{3+} ions in these hosts.

37 The steady state luminescence spectra of $\text{RE}_2\text{O}_2\text{S}$ (RE = Y, La) powders doped with 1% of Ce^{3+} ions are
38 shown in Fig. 7. The excitation spectrum of $\text{Y}_2\text{O}_2\text{S}:\text{Ce}^{3+}$ sample displays two broad bands centered at 265
39 and 407 nm ($\lambda_{em} = 545$ nm). These bands correspond to direct excitation of the Ce^{3+} ions via transitions to
40 the components of Ce^{3+} 5d configuration. The emission spectrum also consists of two lines attributed to
41 allowed 5d–4f transition of Ce^{3+} ion. Generally, emission lines attributed to allowed 5d–4f transition in
42 Ce^{3+} -doped materials are quite broad [51, 52]. Sometimes they are split into two components separated by
43 approximately 2000 cm^{-1} due to the spin-orbit splitting of the $4f^1$ ground state into two components $^2\text{F}_{5/2}$ and
44 $^2\text{F}_{7/2}$. The bands observed in $\text{Y}_2\text{O}_2\text{S}:\text{Ce}^{3+}$ and $\text{La}_2\text{O}_2\text{S}:\text{Ce}^{3+}$ exhibit splitting by 5000 cm^{-1} and cannot be due
45 to splitting of the ground state mentioned above. Therefore, two bands in Ce^{3+} luminescence must be
46 ascribed to the electron transitions from the lowest and second 5d levels to the ground state of Ce^{3+} [53].

1 Change of host to La₂O₂S does not affect spectroscopic properties of Ce³⁺-doped material. The line positions
2 are almost the same for both excitation and emission spectra.

4. Conclusions

3
4
5 In summary, a method for the production of luminescent materials on the basis of rare-earth oxysulfides was
6 developed. The advantage of the method consists in the precipitation of a sulfur-containing precursor from a
7 homogeneous nitrate solution and subsequent transformation in a reducing and sulfidating atmosphere. The
8 use of chemical homogenization made it possible to achieve an excellent uniform distribution of cations in
9 the structure. The use of sulfates as precursors, in view of the presence of sulfur in the structure, greatly
10 simplifies the process of obtaining solid solutions of oxysulfides. All synthesized samples have single phase
11 without any impurities. The excitation and emission spectra of RE₂O₂S:Ln (RE = Y, La; Ln = Dy, Er, Eu)
12 consist of characteristic bands corresponding to the 4f-4f intra configurational transitions. The study of Dy³⁺
13 and Eu³⁺-doped powders revealed that Y₂O₂S host possesses higher local symmetry than La₂O₂S one. The
14 excitation and emission spectra of RE₂O₂S:Ce³⁺ (RE = Y, La) phosphor displayed allowed 5d-4f transition.

Acknowledgement

15
16
17
18 The authors would like to thank the staff of the Engineering Center of the Tyumen State University for their
19 help in carrying out physical and chemical tests. We also thank Andrey Bobylev for conducting electron
20 microscopy.

References

- 21
22
23 [1] Yu.G. Denisenko, A.S. Aleksandrovsky, V.V. Atuchin, A.S. Krylov, M.S. Molokeev, A.S. Oreshonkov,
24 N.P. Shestakov, O.V. Andreev, Exploration of structural, thermal and spectroscopic properties of self-
25 activated sulfate Eu₂(SO₄)₃ with isolated SO₄ groups, *J. Ind. Eng. Chem.* 68 (2018) 109-116.
26 <https://doi.org/10.1016/j.jiec.2018.07.034>
27 [2] Y.G. Denisenko, V.V. Atuchin, M.S. Molokeev, A.S. Aleksandrovsky, A.S. Krylov, A.S.
28 Oreshonkov, S. S. Volkova, O.V. Andreev, Structure, thermal stability, and spectroscopic properties of
29 triclinic double sulfate AgEu(SO₄)₂ with Isolated SO₄ Groups, *Inorg. Chem.*, 57 (21) (2018) 13279-13288.
30 <https://doi.org/10.1021/acs.inorgchem.8b01837>
31 [3] X. Shi, Z. Wang, T. Takei, X. Wang, Q. Zhu, X. Li, B.-N. Kim, X. Sun, J.-G. Li, Selective
32 Crystallization of Four Tungstates (La₂W₃O₁₂, La₂W₂O₉, La₁₄W₈O₄₅, and La₆W₂O₁₅) via Hydrothermal
33 Reaction and Comparative Study of Eu³⁺ Luminescence, *Inorg. Chem.* 57 (11) (2018) 6632-6640.
34 <https://doi.org/10.1021/acs.inorgchem.8b00807>
35 [4] F. Baur, T. Jüstel, Uranyl sensitized Eu³⁺ luminescence in Ln(UO₂)₃(PO₄)₂ O(OH)·6H₂O phosphors (Ln
36 = Y, Eu, La) for warm-white light emitting diodes, *J. Lum.* 196 (2018) 431-436.
37 <https://doi.org/10.1016/j.jlumin.2017.12.073>
38 [5] V.V. Atuchin, A.S. Aleksandrovsky, O.D. Chimitova, T.A. Gavrilova, A.S. Krylov, M.S.
39 Molokeev, A.S. Oreshonkov, B.G. Bazarov, J.G. Bazarova, Synthesis and spectroscopic properties of
40 monoclinic α-Eu₂(MoO₄)₃, *J. Phys. Chem. C.* 118 (28) (2014), 15404-15411.
41 <https://org/doi/10.1021/jp5040739>
42 [6] V.V. Atuchin, A.K. Subanakov, A.S. Aleksandrovsky, B.G. Bazarov, J.G. Bazarova, T.A. Gavrilova,
43 A.S. Krulov, M.S. Molokeev, A.S. Oreshonkov, S.Yu. Stefanovich, Structural and spectroscopic properties
44 of noncentrosymmetric self-activated borate Rb₃EuB₆O₁₂ with B₅O₁₀ units, *Mater. Des.* 140 (2018) 488-494.
45 <https://doi.org/10.1016/j.matdes.2017.12.004>

- [7] J. Lian, F. Liu, J. Zhang, Y. Yang, X. Wang, Z. Zhang, F. Liu, Template-free hydrothermal synthesis of $\text{Gd}_2\text{O}_2\text{SO}_4:\text{Eu}^{3+}$ hollow spheres based on urea-ammonium sulfate (UAS) system, *Optik*. 127 (20) (2016) 8621-8628. <https://doi.org/10.1016/j.ijleo.2016.06.069>
- [8] J. Lian, F. Liu, X. Wang, X. Sun, Hydrothermal synthesis and photoluminescence properties of $\text{Gd}_2\text{O}_2\text{SO}_4:\text{Eu}^{3+}$ spherical phosphor, *Powder Tech.* 253. (2014) 187-192. <https://doi.org/10.1016/j.powtec.2013.11.021>
- [9] Li X., Lian J. Synthesis and characterizations of pompon-like $\text{Y}_2\text{O}_2\text{SO}_4:\text{Eu}^{3+}$ phosphors using a UBHP technique based on UAS system, *Optik*. 127 (1) (2016) 401-406. <https://doi.org/10.1016/j.ijleo.2015.10.091>
- [10] J. Lian, H. Qin, P. Liang, F. Liu, Co-precipitation synthesis of $\text{Y}_2\text{O}_2\text{SO}_4:\text{Eu}^{3+}$ nanophosphor and comparison of photoluminescence properties with $\text{Y}_2\text{O}_3:\text{Eu}^{3+}$ and $\text{Y}_2\text{O}_2\text{S}:\text{Eu}^{3+}$ nanophosphors, *Solid State Sci.* 48 (2015) 147-154. <https://doi.org/10.1016/j.solidstatesciences.2015.08.004>
- [11] H. Jiao, Y. Wang, $\text{Ca}_2\text{Al}_2\text{Si}_2\text{O}_7:\text{Ce}^{3+}, \text{Tb}^{3+}$: A white-light phosphor suitable for whitelight-emitting diodes, *J. Electrochem. Society*, 156 (2009) J117–J120. <http://jes.ecsdl.org/content/156/5/J117.short>
- [12] R. Shrivastava, J. Kaur, V. Dubey, White light emission by Dy^{3+} doped phosphor matrices: A short review, *J. of Fluorescence*. 26 (1) (2016) 105 – 111. <https://doi.org/10.1007/s1089>
- [13] F. Yang, H. Ma, Y. Liu, B. Han, H. Feng, Q. Yu, Photoluminescence properties of novel Dy^{3+} doped $\text{Ba}_5\text{GaAl}_4\text{O}_{12}$ phosphors, *Ceram. Int.* 40 (2014) 10189 – 10192. <https://doi.org/10.1016/j.ceramint.2014.02.068>
- [14] B. M. Cheng, C.K. Duan, P.A. Tanner, Vacuum ultraviolet and visible spectra of Eu^{3+} in $\text{Y}_2\text{O}_2\text{S}$ and $\text{Eu}_2\text{O}_2\text{S}$, *Opt. Mat.* 31 (6) (2009) 902 - 904. <https://doi.org/10.1016/j.optmat.2008.10.036>
- [15] J. Thirumalai, R. Chandramohan, S. Valanarasu, T. A. Vijayan, R. M. Somasundaram, T. Mahalingam, S. R. Srikumar, Shape-selective synthesis and opto-electronic properties of Eu^{3+} -doped gadolinium oxysulfide nanostructures, *J. Mater. Sci.* 44 (14) (2009) 3889-3899. <https://doi.org/10.1007/s10853-009-3531-7>
- [16] X. Lu, L. Yang, Q. Ma, J. Tian, X. Dong, A novel strategy to synthesize $\text{Gd}_2\text{O}_2\text{S}:\text{Eu}^{3+}$ luminescent nanobelts via inheriting the morphology of precursor, *J. Mater. Sci.: Mater. in Electronics*. 25 (12) (2014) 5388-5394. <https://doi.org/10.1007/s10854-014-2317-0>
- [17] S.A. Osseni, S. Lechevallier, M. Verelst, C. Dujardin, J. Dexpert-Ghys, D. Neumeyer, M. Leclercq, H. Baaziz, D. Cussac, V. Santran, R. Mauricot, New nanoplatform based on $\text{Gd}_2\text{O}_2\text{S}:\text{Eu}^{3+}$ core: synthesis, characterization and use for in vitro bio-labelling, *J. Mater. Chem.* 21 (45) (2011) 18365-18372. <https://doi.org/10.1039/C1JM13542B>
- [18] S.A. Osseni, S. Lechevallier, M. Verelst, P. Perriat, J. Dexpert-Ghys, D. Neumeyer, R. Garcia, F. Maye^d, K. Djanashvili, J.A. Peters, E. Magdeleine, H. Gros-Dagnac, P. Celsis, R. Mauricot, Gadolinium oxysulfide nanoparticles as multimodal imaging agents for T 2-weighted MR, X-ray tomography and photoluminescence, *Nanoscale*. 6 (1) (2014) 555-564. <https://doi.org/10.1039/C3NR03982J>
- [19] Q. Zhao, Y. Zheng, N. Guo, Y. Jia, H. Qiao, W. Lv, H. You, 3D-hierarchical $\text{Lu}_2\text{O}_2\text{S}:\text{Eu}^{3+}$ micro/nanostructures: controlled synthesis and luminescence properties, *CrystEngComm*. 14 (20) (2012) 6659-6664. <https://doi.org/10.1039/C2CE25631B>
- [20] Y. Yang, C. Mi, F. Yu, X. Su, C. Guo, G. Li, J. Zhang, L. Liu, Y. Liu, X. Li, Optical thermometry based on the upconversion fluorescence from $\text{Yb}^{3+}/\text{Er}^{3+}$ codoped $\text{La}_2\text{O}_2\text{S}$ phosphor, *Ceram. Int.* 40 (7 Part A) (2014) 9875-9880. <https://doi.org/10.1016/j.ceramint.2014.02.081>
- [21] S. Yokono, T. Abe, T. Hoshina, Red luminescence of Ce^{3+} to the large stokes shifts in $\text{Y}_2\text{O}_2\text{S}$ and $\text{Lu}_2\text{O}_2\text{S}$, *J. Lum.* 24/25 (Part 1) (1981) 309-312. [https://doi.org/10.1016/0022-2313\(81\)90279-9](https://doi.org/10.1016/0022-2313(81)90279-9)
- [22] Y. Yang, C. Mi, F. Yu, X. Su, C. Guo, G. Li, J. Zhang, L. Liu, Y. Liu, X. Li, Optical thermometry based on the upconversion fluorescence from $\text{Yb}^{3+}/\text{Er}^{3+}$ codoped $\text{La}_2\text{O}_2\text{S}$ phosphor // *Ceram. Int.* 2014. V. 40. № 7, Part A. P. 9875-9880. <https://doi.org/10.1016/j.ceramint.2014.02.081>

- [23] X. Wang, Z. Zhang, Z. Tang, Y. Lin, Characterization and properties of a red and orange Y₂O₂S-based long afterglow phosphor, *Mater. Chem. Phys.* 80 (2003) 1-5. [https://doi.org/10.1016/S0254-0584\(02\)00097-4](https://doi.org/10.1016/S0254-0584(02)00097-4)
- [24] G.A. Kumar, M. Pokhrel, A. Martinez, R.C. Dennis, I.L. Villegas, D.K. Sardar, Synthesis and spectroscopy of color tunable Y₂O₂S:Yb³⁺, Er³⁺ phosphors with intense emission, *J. Alloy. Compd.* 513 (2012) 559 – 565. <https://doi.org/10.1016/j.jallcom.2011.11.006>
- [25] T.W. Chou, S. Mylswamy, R.S. Liu, S.Z. Chuang, Eu substitution and particle size control of Y₂O₂S for the excitation by UV light emitting diodes, *Solid State Comm.* 136 (2005) 205 – 209. <https://doi.org/10.1016/j.ssc.2005.07.032>
- [26] H. Wang, M. Xing, X. Luo, X. Zhou, Y. Fu, T. Jiang, Y. Peng, Y. Ma, X. Duan, Up-conversion emission colour modulation of Y₂O₂S:Yb, Er under 1.55 μm and 980 nm excitation, *J. Alloy. Compd.* 587 (2014) 344 – 348. <https://doi.org/10.1016/j.jallcom.2013.10.163>
- [27] Yu.G. Denisenko, N.A. Khritokhin, O.V. Andreev, S.A. Basova, E.I. Sal'nikova, A.A. Polkovnikov, Thermal decomposition of europium sulfates Eu₂(SO₄)₃·8H₂O and EuSO₄, *J. Solid State Chem.* 255 (2017) 219 – 224. <https://doi.org/10.1016/j.jssc.2017.08.020>
- [28] H. Stark, R.L.N. Yatavelli, S. L. Thompson, H. Kang, J. E. Krechmer, J. R. Kimmel, B.B. Palm, W. Hu, P.L. Hayes, D.A. Day, P. Campuzano-Jost, M.R. Canagaratna, J.T. Jayne, D.R. Worsnop, J.L. Jimenez, Impact of thermal decomposition on thermal desorption instruments: advantage of thermogram analysis for quantifying volatility distributions of organic species, *Environ. Sci. Technol.* 51 (15) (2017) 8491–8500. <https://doi.org/10.1021/acs.est.7b00160>
- [29] O.V. Andreev, I.A. Razumkova, A.N. Boiko. Synthesis and thermal stability of rare earth compounds RE₃F₃, RE₃·nH₂O and (H₃O)RE₃F₁₀·nH₂O (RE= Tb– Lu, Y), obtained from sulfide precursors, *J. Fluor. Chem.* 207(2018)77-83. <https://doi.org/10.1016/j.jfluchem.2017.12.001>
- [30] I.A. Razumkova, Synthesis of NaYF₄ compounds from sulfide precursors, *J. Fluor. Chem.* 205(2018) 1-4. <https://doi.org/10.1016/j.jfluchem.2017.10.012>
- [31] M. Unni, A.M. Uhl, S. Savliwala, B.H. Savitzky, R. Dhavalikar, N. Garraud, D.P. Arnold, L.F. Kourkoutis, J.S. Andrew, C. Rinaldi, Thermal decomposition synthesis of iron oxide nanoparticles with diminished magnetic dead layer by controlled addition of oxygen, *ACS Nano.* 11 (2) (2017) 2284 – 2303. <https://doi.org/10.1021/acs.nano.7b00609>
- [32] S.A. Osseni, Yu.G. Denisenko, J.K. Fatombi, E.I. Sal'nikova, O.V. Andreev, Synthesis and characterization of Ln₂O₂SO₄ (Ln= Gd, Ho, Dy and Lu) nanoparticles obtained by coprecipitation method and study of their reduction reaction under H₂ flow, *J. Nanostr. Chem.* 7 (4) (2017) 337 – 343. <https://doi.org/10.1007/s40097-017-0243-4>
- [33] P.O. Andreev, E.I. Sal'nikova, O.V. Andreev, Yu.G. Denisenko, I.M. Kovenskii, Synthesis and Upconversion Luminescence Spectra of (Y_{1-x-y}Yb_xEr_y)₂O₂S, *Inorg. Mater.* 53 (2) (2017) 200 – 206. <https://doi.org/10.1134/S0020168517020029>
- [34] P.O. Andreev, E.I. Sal'nikova, I.M. Kovenski, Preparation of Ln₂O₂S (Ln = Gd, Dy, Y, Er, Lu) in flowing hydrogen and hydrogen sulfide, *Inorg. Mater.* 50 (2014) 1018 – 1023. <https://doi.org/10.1134/S0020168517020029>
- [35] O.V. Andreev, Yu.G. Denisenko, E.I. Sal'nikova, N.A. Khritokhin, K.S. Zyryanova, Specifics of Reactions of Cerium Sulfate and Europium Sulfate with Hydrogen, *Russ. J. Inorg. Chem.* 61 (2016) 296 – 301. <https://doi.org/10.1134/S0036023616030025>
- [36] P.O. Andreev, E.I. Sal'nikova, O.V. Andreev, I.M. Kovenskii, Kinetic Schemes of Chemical Transformations and Particle Morphology upon Interaction between Ln₂(SO₄)₃ (Ln = La, Pr, Nd, Sm) and Hydrogen // *Russ. J. Phys. Chem. A.* 90 (1) (2016) 25 –30. <https://doi.org/10.1134/S0036024416010027>

- [37] E.I. Sal'nikova, P.O. Andreev, S.M. Antonov, Kinetic Diagrams of $\text{Ln}_2\text{O}_2\text{SO}_4$ Phase Transformations in a H_2 Flow ($\text{Ln} = \text{La}, \text{Pr}, \text{Nd}, \text{Sm}$), *Russ. J. Phys. Chem. A.* 87 (8) (2013) 1280 – 1283.
<https://doi.org/10.1134/S0036024413080207>
- [38] P.O. Andreev, E.I. Sal'nikova, A.A. Kislitsyn, Kinetics of the transformation of $\text{Ln}_2\text{O}_2\text{SO}_4$ into $\text{Ln}_2\text{O}_2\text{S}$ ($\text{Ln} = \text{La}, \text{Pr}, \text{Nd}, \text{Sm}$) in a hydrogen flow, *Russ. J. Phys. Chem. A.* 87 (9) (2013) 1482 – 1487.
<https://doi.org/10.1134/S0036024413080050>
39. Bruker AXS TOPAS V4: General profile and structure analysis software for powder diffraction data. User's Manual. Bruker AXS, Karlsruhe, Germany. 2008.
- [40] J. Kuang, Y. Liu, J. Zhang, White-light-emitting long-lasting phosphorescence in Dy^{3+} -doped SrSiO_3 , *J. Solid State Chem.* 179 (2006) 266 – 269. <https://doi.org/10.1016/j.jssc.2005.10.025>
- [41] P. Babu, K.H. Jang, E.S. Kim, L. Shi, H.J. Seo, F. Rivera-López, U.R. Rodriguez-Mendoza, V. Lavin, R. Vijaya, C.K. Jayasankar L.R. Moorthy, Spectral investigations on Dy^{3+} -doped transparent oxyfluoride glasses and nanocrystalline glass ceramics, *J. Appl. Phys.* 105 (2009) 13516.
<https://doi.org/10.1063/1.3021451>
- [42] I.E. Kolesnikov, A.A. Kalinichev, M.A. Kurochkin, E.V. Golyeva, A.S. Terentyeva, E.Yu. Kolesnikov, E. Lähderanta, Structural, luminescence and thermometric properties of nanocrystalline YVO_4 : Dy^{3+} temperature and concentration series, *Sci. reports.* 9 (1) (2019) 2043. <https://doi.org/10.1038/s41598-019-38774-6>
- [43] I.E. Kolesnikov, A.V. Povolotskiy, D.V. Mamonova, E.Y. Kolesnikov, A.V. Kurochkin, E. Lähderanta, M.D. Mikhailov, Asymmetry ratio as a parameter of Eu^{3+} local environment in phosphors, *J. Rare Earths.* 36 (2018) 474 – 481. <https://doi.org/10.1016/j.jre.2017.11.008>
- [44] E. Oomen, A.-M.A. Van Dongen, Europium (III) in oxide glasses: dependence of the emission spectrum upon glass composition, *J. Non. Cryst. Solids.* 111 (1989) 205-213. [https://doi.org/10.1016/0022-3093\(89\)90282-2](https://doi.org/10.1016/0022-3093(89)90282-2)
- [45] U. Fawad, H.J. Kim, S. Khan, M. Khan, L. Ali, Photoluminescent properties of white-light-emitting $\text{Li}_6\text{Y}(\text{BO}_3)_3:\text{Dy}^{3+}$ phosphor, *Solid State Sci.* 62 (2016) 1–5.
<https://doi.org/10.1016/j.solidstatesciences.2016.08.008>
- [46] Y.A. Dolinskaya, I.E. Kolesnikov, A.V. Kurochkin, A.A. Man'shina, M.D. Mikhailov, and A.V. Semench, Sol-gel synthesis and luminescent properties of $\text{YVO}_4:\text{Eu}$ nanoparticles, *Glass Phys. Chem.* 39 (3) (2013) 308 – 310. <https://doi.org/10.1134/S1087659613030061>
- [47] I.E. Kolesnikov, A.V. Povolotskiy, D.V. Tolstikova, A.A. Manshina, M.D. Mikhailov, Luminescence of $\text{Y}_3\text{Al}_5\text{O}_{12}:\text{Eu}^{3+}$ nanophosphors in blood and organic media, *J. Phys. D.* 48 (7) (2015) 075401. <https://doi.org/10.1088/0022-3727/48/7/075401/meta>
- [48] I.E. Kolesnikov, D.V. Mamonova, E. Lähderanta, A.V. Kurochkin, M.D. Mikhailov, The impact of doping concentration on structure and photoluminescence of $\text{Lu}_2\text{O}_3:\text{Eu}^{3+}$ nanocrystals, *J. Lum.* 187 (2017) 26 – 32. <https://doi.org/10.1016/j.jlumin.2017.03.006>
- [49] Q. Dai, H. Song, M. Wang, X. Bai, B. Dong, R. Qin, X. Qu, H. Zhang, Size and Concentration Effects on the Photoluminescence of $\text{La}_2\text{O}_2\text{S}:\text{Eu}^{3+}$ Nanocrystals, *J. Phys. Chem. C.* 112 (49) (2008) 19399-19404. <https://doi.org/10.1021/jp808343f>
- [50] R.H. Krauss, R.G. Hellier, J.C. McDaniel, Surface temperature imaging below 300 K using $\text{La}_2\text{O}_2\text{S}:\text{Eu}$, *Appl. Opt.* 33 (18) (1994) P. 3901 – 3904. <https://doi.org/10.1364/AO.33.003901>
- [51] M. Upasani, B. Butey, S.V. Moharil, Synthesis, characterization and optical properties of $\text{Y}_3\text{Al}_5\text{O}_{12}:\text{Ce}$ phosphor by mixed fuel combustion synthesis, *J. Alloy. Compd.* 650 (2015) 858 – 862.
<https://doi.org/10.1016/j.jallcom.2015.08.076>

- 1 [52] H.-L. Li, X.-J. Liu, L.-P. Huang, Luminescent properties of LuAG:Ce phosphors with different Ce
2 contents prepared by a sol-gel combustion method, *Opt. Mater. (Amst)*. 29 (2007) 1138–1142.
3 <https://doi.org/10.1016/j.optmat.2006.05.002>
4 [53] J.-J. Zhao, C.-X. Guo, R.-W. Guo, J.-T. Hu, Red luminescence of $\text{Lu}_2\text{O}_2\text{S}:\text{Ce}$ and $\text{Y}_2\text{O}_2\text{S}:\text{Ce}$ at room
5 temperature, *J. Alloy. Compd.* 436 (2007) 174–177. <https://doi.org/10.1016/j.jallcom.2006.06.103>
6
7

8 Captions

9 Fig.1. Experimental, calculated, and difference Rietveld plot of: a,b) $(\text{RE}_{0.99}\text{Ln}_{0.01})_2(\text{SO}_4)_3$; c,d)
10 $(\text{RE}_{0.99}\text{Ln}_{0.01})_2(\text{SO}_4)_3 - (\text{RE}_{0.99}\text{Ln}_{0.01})_2\text{O}_2\text{SO}_4 - (\text{RE}_{0.99}\text{Ln}_{0.01})_2\text{O}_2\text{S} - (\text{RE}_{0.99}\text{Ln}_{0.01})_2\text{O}_3$; e,f) $(\text{RE}_{0.99}\text{Ln}_{0.01})_2\text{O}_2\text{S} -$
11 $(\text{RE}_{0.99}\text{Ln}_{0.01})_2\text{O}_3$; g,h) $(\text{RE}_{0.99}\text{Ln}_{0.01})_2\text{O}_2\text{S}$.

12 Fig. 2. SEM image of a) $(\text{La}_{0.99}\text{Dy}_{0.01})_2(\text{SO}_4)_3$; b) $(\text{La}_{0.99}\text{Dy}_{0.01})_2\text{O}_2\text{S}$

13 Fig. 3. Coordination polyhedron structure $\text{La}_2\text{O}_2\text{S}$

14 Fig. 4. Excitation and emission spectra of $\text{Y}_2\text{O}_2\text{S}:\text{Dy}^{3+}$ and $\text{La}_2\text{O}_2\text{S}:\text{Dy}^{3+}$ phosphors

15 Fig. 5. Excitation and emission spectra of $\text{Y}_2\text{O}_2\text{S}:\text{Er}^{3+}$ and $\text{La}_2\text{O}_2\text{S}:\text{Er}^{3+}$ phosphors

16 Fig. 6. Excitation and emission spectra of $\text{Y}_2\text{O}_2\text{S}:\text{Eu}^{3+}$ and $\text{La}_2\text{O}_2\text{S}:\text{Eu}^{3+}$ phosphors

17 Fig. 7. Excitation and emission spectra of $\text{Y}_2\text{O}_2\text{S}:\text{Ce}^{3+}$ and $\text{La}_2\text{O}_2\text{S}:\text{Ce}^{3+}$ phosphors

1
2
3

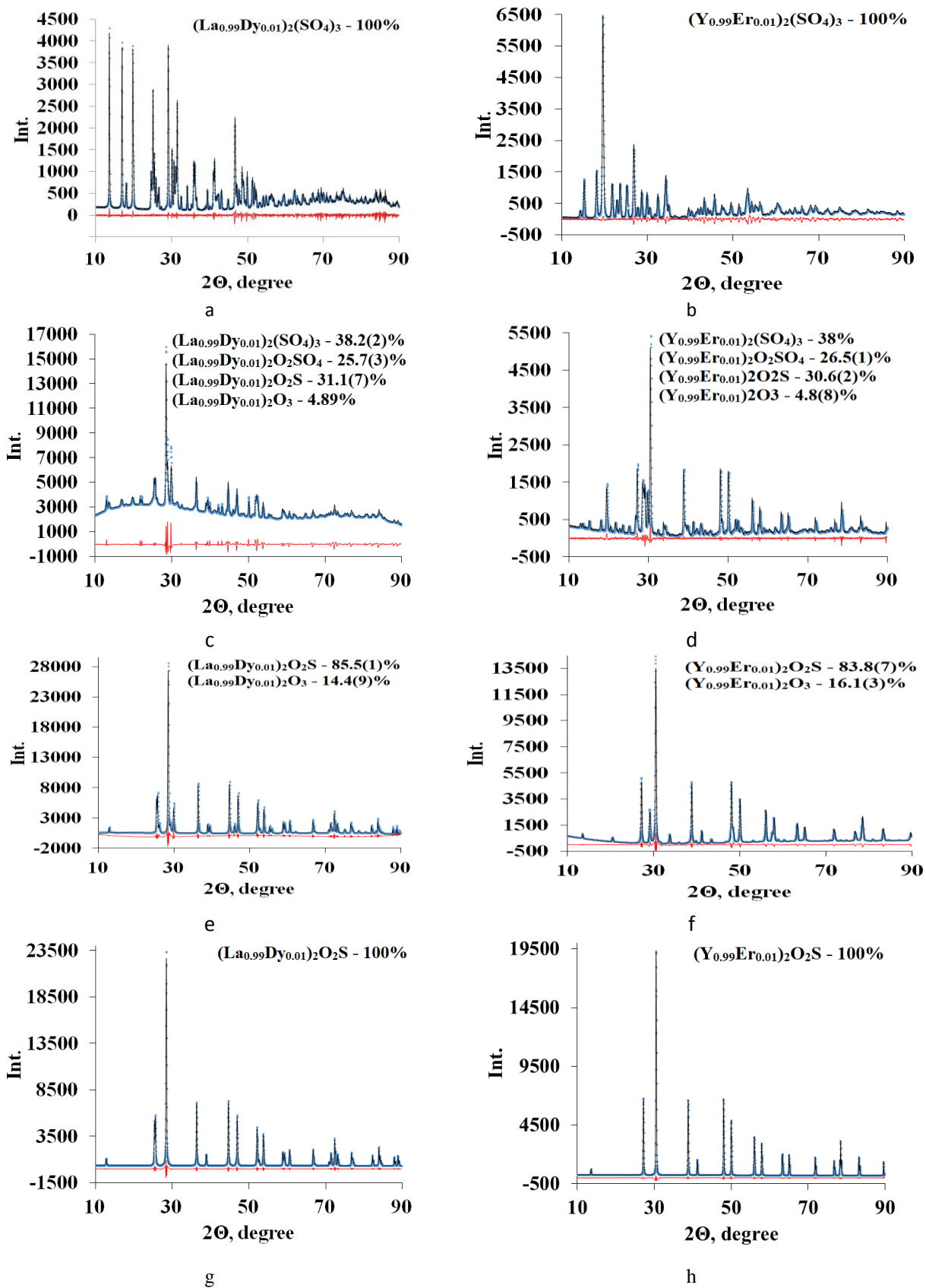
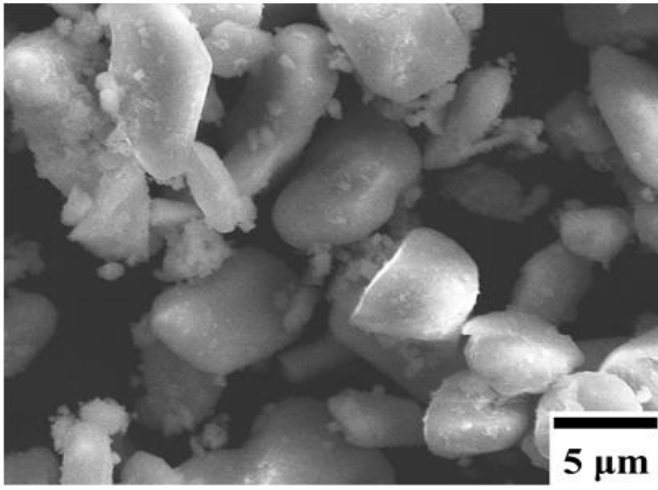
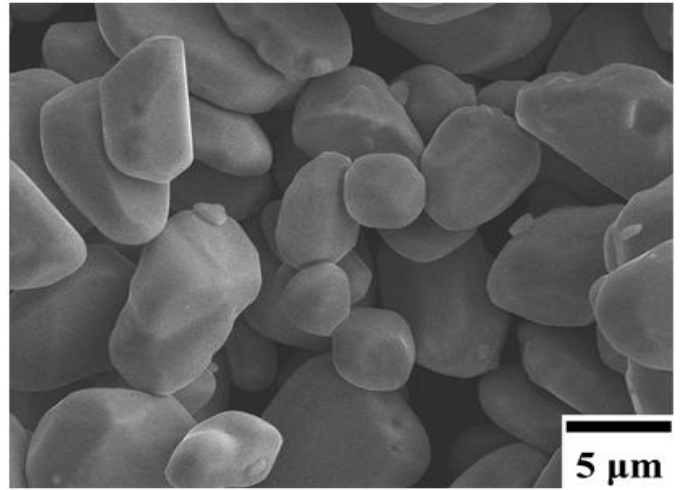


Fig. 1

4



a)



b)

Fig. 2

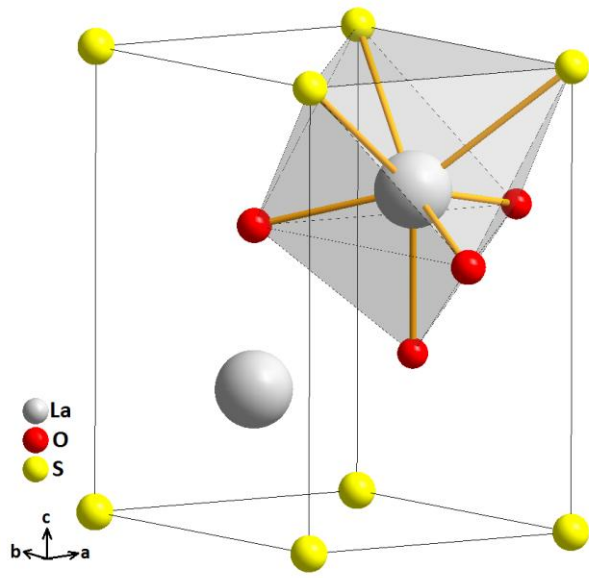


Fig. 3.

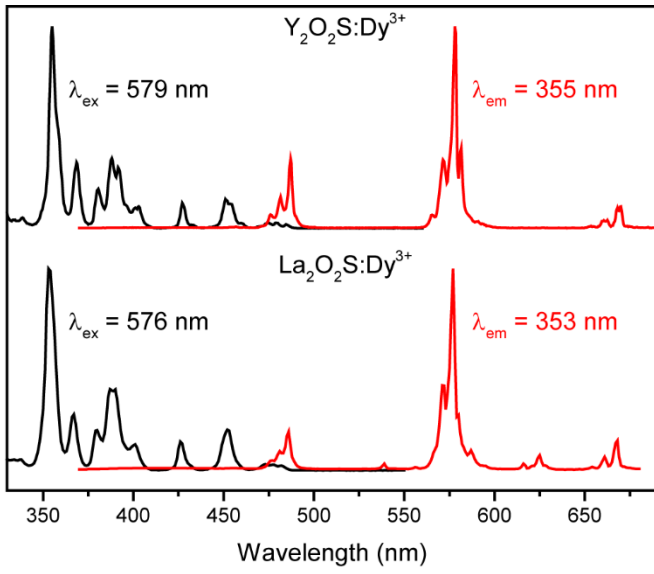


Fig. 4

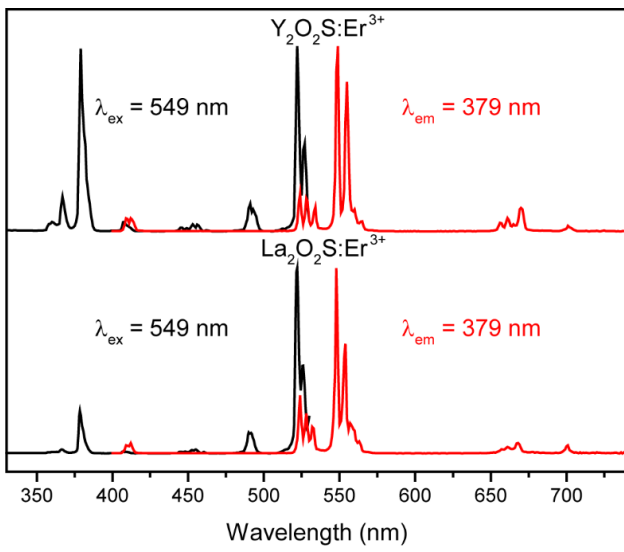


Fig. 5

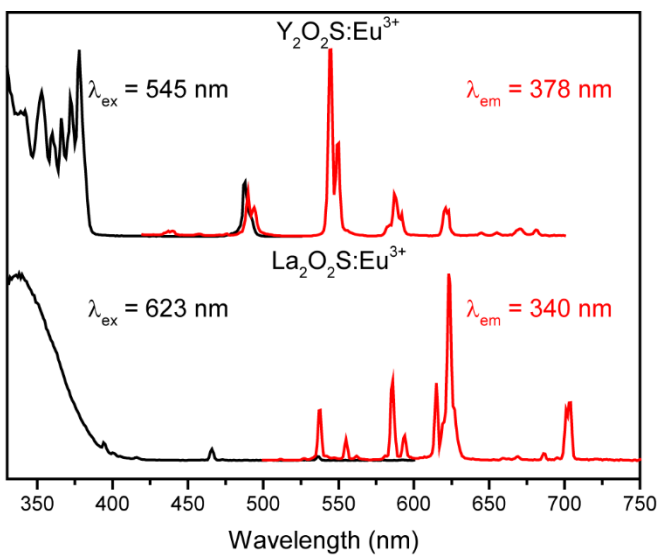
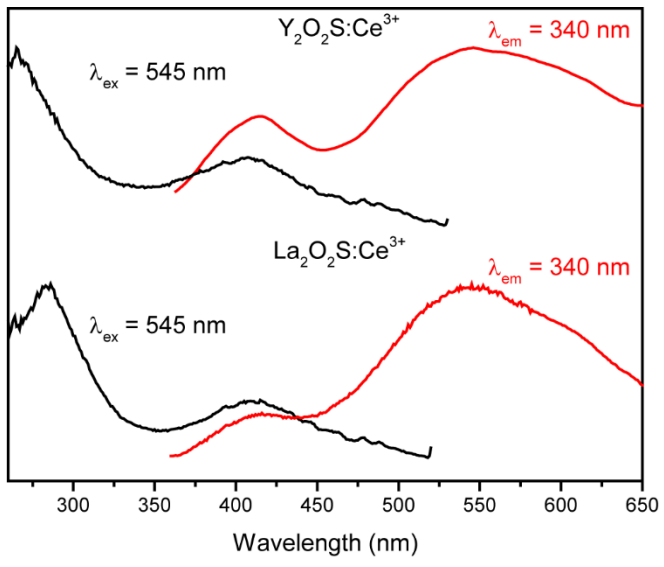


Fig. 6



1
2 Fig. 7

1 Corresponding author: E.I. Sal'nikova
2 Tyumen State University, Tyumen 625003, Russia
3 E-mail: elenasalnikova213@gmail.com
4

5 **Synthesis and Optical Properties RE₂O₂S:Ln (RE = La, Y; Ln = Ce, Eu, Dy, Er)**

6
7 E.I. Sal'nikova^{1,2}, Yu.G. Denisenko³, A.S. Aleksandrovsky^{4,5}, I.E. Kolesnikov^{6,7}, E. Lähderanta⁷,
8 P.O. Andreev¹, N.O. Azarapin¹, O.V. Andreev¹, S.A. Basova¹, A.V. Matigorov¹
9

10 ¹Department of Inorganic and Physical Chemistry, Tyumen State University, Tyumen 625003, Russia

11 ²Department of General Chemistry, Northern Trans-Ural Agricultural University, Tyumen, 625003, Russia

12 ³Department of General and Special Chemistry, Industrial University of Tyumen, Tyumen 625000, Russia

13 ⁴Laboratory of Coherent Optics, Kirensky Institute of Physics Federal Research Center KSC SB RAS,
14 Krasnoyarsk 660036, Russia

15 ⁵Institute of Nanotechnology, Spectroscopy and Quantum Chemistry, Siberian Federal University,
16 Krasnoyarsk 660041, Russia

17 ⁶Center for Optical and Laser Materials Research, St. Petersburg State University, St. Petersburg 199034,
18 Russia

19 ⁷Department of Physics, Lappeenranta University of Technology LUT, Lappeenranta 53850, Finland
20
21

22 **Abstract**

23 The phase formation sequence was studied in the preparation of solid solutions of RE₂O₂S: Ln' (RE = La, Y;
24 Ln' = Ce, Eu, Dy, Er) by the reduction of the match co-precipitated sulfates, followed by sulfidization of the
25 reduction products. For uniform distribution of cations in the matrix, a method of chemical homogenization
26 was used, consisting in the preparation of an aqueous solution containing all the necessary cations and their
27 subsequent precipitation in the form of sulfates. The use of sulfates as precursors facilitates the process of
28 obtaining solid solutions of oxysulfides, since sulfates already contain SO₄²⁻-ions. The phase and
29 morphological certification of the obtained solid solutions was carried out. The study of steady state
30 luminescent properties demonstrated characteristic bands which are assigned to 4*f*-4*f* and 5*d*-4*f* transition.
31 The obtained results showed the possibility of applying the method to synthesize optical ceramics based on
32 solid solutions RE₂O₂S: Ln (RE = La, Y; Ln = Ce, Eu, Dy, Er).
33
34

35 **Keywords:** oxysulfides, sulfates, rare-earth, reduction, optical ceramic, luminescence
36

37 **1. Introduction**

38 Oxygen-containing compounds of rare-earth elements have long attracted the attention of researchers
39 due to their effective luminescent properties, which have found application in many optical systems [1-
40 6]. Despite the fact that the luminescence is mainly determined by the nature of the substituting ion, the host
41 matrix into which this ion is embedded influences on the emission lines intensity through its crystal field [7-
42 10]. Lanthanide ions can emit light in the near UV, visible and infrared regions of the spectrum. Each ion
43 has a characteristic absorption and emission spectrum. Ln³⁺ radiation is characterized by high color purity;
44 therefore, materials activated by lanthanides are attractive for creating LEDs, fluorescent lamps, plasma
45 displays, and active media for solid-state lasers [11-13].

46 Activated materials based on oxysulfides of rare-earth elements are widely used in various fields [14-
47 22]. However, in recent years, only laborious, poorly reproducible methods of producing nanoparticles are

described in the literature for these objects. At the same time, the need for relatively simple synthesis methods allowing large batches of optical ceramics does not decrease[23–27].

Thermal decomposition methods are convenient for obtaining materials with different properties [28–32]. In the preparation of oxysulfides, particular attention is drawn to methods for reducing sulfur containing compounds to higher oxidation degrees. Compared with solid-phase methods, the recovery method differs in manufacturability, reproducibility, and the ability to produce several tens of grams of a product at once [33–39].

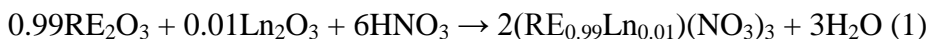
Thus, the aim of the work is to study the chemistry of reactions in the sequential processing of co-precipitated sulfates of rare earth elements in the atmosphere of H₂, H₂S to obtain activated oxysulfides and investigate the morphology of the obtained reaction products and their luminescent properties.

2. Materials and methods

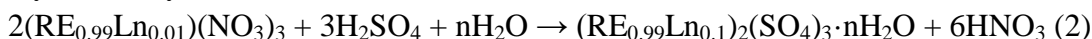
2a. Preparative Methods

Powders of co-precipitated sulfates were obtained by precipitation from a nitrate solution with concentrated sulfuric acid. For the synthesis, high purity reagents were used: Ln₂O₃ (≥99.99%, ultrapure, TDM-96 Ltd. Russia). Concentrated nitric acid solution (C(HNO₃) = 14.6 mol/L, ultrapure, Vekton Ltd., Russia), concentrated sulfuric acid solution (C (H₂SO₄) = 17.9 mol/L, ultrapure, Vekton Ltd., Russia). Weighing was carried out on an analytical balance with an accuracy of 0.1 mg. Before weighing, the oxides were calcined in a muffle furnace at a temperature of 1000°C for 12 hours to remove sorbed gases and products of their interaction with oxides (Ln(OH)₃, Ln₂(CO₃)₂). Acid solutions were measured using glass measuring cylinders with an accuracy of 0.1 ml.

The calculated weighed amount of oxides with a total weight of 5.0 g was placed in a 100 mL glass round-bottom flask, then 7.0 mL of a concentrated solution of nitric acid was poured in small portions. The reaction mixture was heated on a mantle until the oxides were completely dissolved. As a result, a nitrate solution was obtained with evenly distributed cations:



After cooling the solution, 3.0 ml of concentrated sulfuric acid was poured in small portions to it, avoiding strong heating of the reaction mixture. As a result, a precipitate of co-precipitated sulfates and their crystalline hydrates forms:



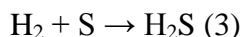
After carrying out the precipitation reaction, the reaction mixture is distilled off to the dry residue. The obtained polycrystalline product is additionally calcined in a tubular furnace at a temperature of 500°C to remove sorbed moisture and acids. Later, the powder is annealed at the same temperature for 7 days, in order to form an acceptable crystallite structure.

This method of chemical homogenization has a number of significant advantages:

- In the process of synthesis, no cations other than Ln³⁺ are added to the reaction mixture, which excludes their replacement and the formation of defects in the crystal structure.
- Sulfates precipitate from a homogeneous nitrate solution, which ensures high stoichiometry and uniform distribution of cations within the crystal lattice.
- Conducting the reaction in an environment of concentrated sulfuric acid allows to form the structure of anhydrous sulfate at the earliest stages.

The reduction of sulfates in a hydrogen atmosphere was carried out on the apparatus shown in Figure S1. High purity hydrogen was obtained by the electrolytic method in the SPECTR - 6M hydrogen generator. The temperature in the furnace was set using a microprocessor controller. The temperature in the furnace was controlled using chromel-alumel thermocouple. A weighed amount of co-precipitated sulfates was placed in a quartz reactor, and for 30 minutes it was purged with hydrogen from a generator at a rate of 6

L/h. After that, the reactor was placed in a heated vertical furnace and kept for the required amount of time. After completion of the process, the reactor was removed from the furnace and cooled to room temperature. Processing of the reduced products in an atmosphere of hydrogen sulfide was carried out on a similar setup (Fig. S2). The difference lies in the fact that before being fed into the reactor, the hydrogen passes through a flask with molten elemental sulfur and heated to 350 °C. As a result, hydrogen sulfide is formed:



Consequently, it is not a hydrogen inflows the reactor, but a hydrogen sulfide.

2b. Methods of physical-chemical analysis

X-ray phase analysis (XRD) was performed on a BRUKER D2 PHASER diffractometer with a linear detector LYNXEYE (CuK α radiation, Ni-filter). Rietveld refinement of all six samples was performed by using TOPAS 4.2 [40]. Almost all peaks were indexed.

Electron-microscopic analysis was carried out on electron microscope JEOL JSM-6510LV. X-ray energy-dispersive analyzer was used to register X-rays at element spectrum plotting in selected sample surface areas. The inaccuracy in element content determination was equal to $\pm 0.2\%$.

All measurements of the luminescent properties were carried out on a research-grade spectrofluorimeter. Horiba JobinYvon Fluorolog-3 equipped with double monochromators for excitation and emission channels and 450 W xenon lamp as an excitation source.

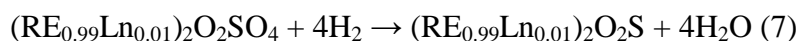
3. Result and Discussion

3a. Synthetic experiment

Detailed consideration of the chemical transformations taking place during the transformation of co-precipitated sulfates into the corresponding solid solutions of oxysulfides was made on the basis of two model systems La₂(SO₄)₃:Dy³⁺ and Y₂(SO₄)₃:Er³⁺. The results obtained were used to synthesize all other solid solutions, which are reported in this work.

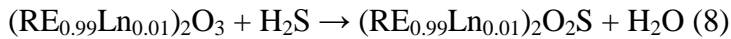
The carrying out of the co-precipitation of sulfates and the subsequent annealing led to the formation of structures of solid solutions of sulfates in which the doping ion is fully incorporated into the crystal lattice of the matrix and occupies the crystallographic positions of the host cation. According to X-ray diffraction data, all samples of co-precipitated sulfates are single-phase (Fig. 1a, b). There is a slight shift in the unit cell parameters caused by the difference in the radii of the cations of the matrix and the dopant.

The appearance of gaseous reduction products was recorded at a temperature of 570°C. In this connection, sulfate reduction was carried out at $t = 600^\circ\text{C}$. At this temperature, after 60 minutes of the process, the products mainly consist of 4 phases: (RE_{0.99}Ln_{0.01})₂(SO₄)₃ - (RE_{0.99}Ln_{0.01})₂O₂SO₄ - (RE_{0.99}Ln_{0.01})₂O₂S - (RE_{0.99}Ln_{0.01})₂O₃ (Fig. 1c, d). There was an incomplete transformation of the initial sulfates into the reaction products. The following chemical equations correspond to the formation of the corresponding reduction products:



After 10 hours of carrying out the process at a given temperature, polycrystalline products consist of two phases: (RE_{0.99}Ln_{0.01})₂O₂S, (RE_{0.99}Ln_{0.01})₂O₃ (Fig. 1 e, f). The absence of compounds containing sulfur in the highest degree of oxidation of in the synthesis products indicates on a complete redox transformation. In all samples, the phase output (RE_{0.99}Ln_{0.01})₂O₂S was not lower than 80%. Thus, the stage of sulfate reduction in a hydrogen atmosphere allows the formation of two-phase polycrystalline intermediates with a predominant content of the oxysulfide phase, which should greatly facilitate the sulfidation procedure.

1 The interaction of two-phase intermediates with hydrogen sulfide at a temperature of 800 ° C for 5 hours
2 leads to the formation of single-phase powders (RE_{0.99}Ln_{0.01})₂O₂S (Fig. 1 g, h). The transformation
3 corresponds to the transformation of the oxide phase to the oxysulfide under the action of a mild sulfiding
4 agent H₂S:



5 Sulfate powders, formed predominantly by loose agglomerates (Fig. 2, a) with sizes up to 10 μm. The
6 resulting oxysulfide powders have a more distinct cut shape, a denser structure and a uniform size
7 distribution (Fig. 2, a). The morphological transformation is evidently due to the elevated temperatures and
8 the diffusion character of the reduction and sulfidation processes.

9
10 The enlargement obviously occurs as a result of the desire of the system to lower its energy. What
11 corresponds to a decrease in the surface area of the polycrystalline samples. Particle cutting appears as a
12 result of high rates of chemical reactions and rapid mass transfer. The indicated tendency to particle
13 aggregation is often observed during similar processes [27, 32-35].

14 **3b. Structural and spectroscopic properties**

15 Crystal structure of both hosts belongs to *P-3m 1* space group of trigonal symmetry class. Y and La occupy a
16 single inequivalent site. In both oxysulfides the local environment of them is a distorted polyhedron with
17 seven vertices, four of them being oxygen ions and three being sulfur ions. Layered structure of oxysulfides
18 implies that sulfur and oxygen are positioned in opposite hemispheres of the local environment of either Y
19 or La. Rare-earth doping ions are expected to occupy Y and La sites, and their local environment is
20 determined by the structure host, with the local symmetry C_{3v}. Therefore, absence of inversion symmetry
21 must be pronounced in optical spectra of doping ions. Variation of luminescence properties of doping RE
22 ions in one host with respect to another is usually ascribed to the change of the extent of inversion symmetry
23 violation. Examining the geometry of local environment of RE ion in Y₂O₂S and La₂O₂S (Fig. 3) we observe
24 that both environments are geometrically identical.

25 The excitation and emission spectra of RE₂O₂S (RE = Y, La) activated by 1% of Dy³⁺ ions are shown in
26 Fig. 4. The observed spectra exhibit characteristic intra-configurational 4f-4f transitions. Excitation
27 spectrum of Y₂O₂S:Dy³⁺ monitored at 579 nm (⁴F_{9/2}-⁶H_{13/2}), displays following transitions: ⁶H_{15/2}-⁴P_{7/2} (355
28 nm), ⁶H_{15/2}-⁴P_{5/2} (369 nm), ⁶H_{15/2}-⁴I_{13/2} (388 nm), ⁶H_{15/2}-⁴G_{11/2} (427 nm), ⁶H_{15/2}-⁴I_{15/2} (451 nm) and ⁶H_{15/2}-
29 ⁴F_{9/2} (479 nm). The emission spectrum Y₂O₂S:Dy³⁺ sample is dominated by green-yellow band (579 nm)
30 corresponding to the hypersensitive ⁴F_{9/2}-⁶H_{13/2} transition. Other observed lines are attributed to the ⁴I_{15/2}-
31 ⁶H_{15/2} (457 nm), ⁴F_{9/2}-⁶H_{15/2} (487 nm), and ⁴F_{9/2}-⁶H_{11/2} (670 nm) transitions. It is well-known that ⁴F_{9/2}-⁶H_{13/2}
32 is the forced electric dipole transition, which is hypersensitive and its intensity can vary by orders of
33 magnitude depending on the local site symmetry, whereas ⁴F_{9/2}-⁶H_{15/2} transition intensity is insignificantly
34 affected by the environment [40-42]. The excitation and emission spectra of La₂O₂S:Dy³⁺ are similar to the
35 Y₂O₂S:Dy³⁺ ones. Small blue shift of bands and redistribution between them were observed. So, the most
36 prominent transitions in excitation and emission spectra of La₂O₂S:Dy³⁺ are centered at 353 and 576 nm,
37 respectively. Observed luminescence spectra of Dy ion are consistent with the concept that they occupy
38 Y(La) sites with the local symmetry C_{3v}.

39 To compare the crystal structure and crystal field of Y₂O₂S:Dy³⁺ and La₂O₂S:Dy³⁺ powders, we calculated
40 ratio (*R*_{Dy}) between ⁴F_{9/2}-⁶H_{13/2} and ⁴F_{9/2}-⁶H_{15/2} intensities. This parameter is similar to the well-known
41 asymmetry ratio for Eu³⁺ ions [43, 44]. *R*_{Dy} value give information about the local surrounding and
42 environmental changes near the Dy³⁺ ions. The higher the calculated parameter is, the more apart from a
43 centrosymmetric geometry luminescent center is located. It is well-known that if Dy³⁺ is located at low
44 symmetry without the inversion symmetry, the yellow emission is the most intense of all the transitions, as
45 is the case with our synthesized nanocrystalline phosphors [45]. Experimental *R*_{Dy} values for Y₂O₂S:Dy³⁺
46

1 and $\text{La}_2\text{O}_2\text{S}:\text{Dy}^{3+}$ samples are 3.13 and 4.65. In view of geometrical identity of local environments, this
2 difference must be ascribed to the interplay between ionic radii of Y and La and the unit cell parameters, i.e.
3 closer ligands at the same degree of inversion symmetry violation.

4 The steady state luminescence spectra of $\text{RE}_2\text{O}_2\text{S}$ (RE = Y, La) powders doped with 1% of Er^{3+} ions are
5 presented in Fig. 5. The excitation spectrum of $\text{Y}_2\text{O}_2\text{S}:\text{Er}^{3+}$ was monitored at 549 nm ($^4\text{F}_{9/2}-^4\text{I}_{15/2}$) within
6 spectral range of 330–530 nm. It consists of $^4\text{I}_{15/2}-^4\text{G}_{7/2}$ (360 nm), $^4\text{I}_{15/2}-^4\text{G}_{9/2}$ (367 nm), $^4\text{I}_{15/2}-^4\text{G}_{11/2}$ (379
7 nm), $^4\text{I}_{15/2}-^2\text{H}_{9/2}$ (408 nm), $^4\text{I}_{15/2}-^4\text{F}_{3/2}$ (446 nm), $^4\text{I}_{15/2}-^4\text{F}_{5/2}$ (453 nm), $^4\text{I}_{15/2}-^4\text{F}_{7/2}$ (491 nm), and $^4\text{I}_{15/2}-^2\text{H}_{11/2}$
8 (522 nm). The emission spectrum includes narrow bands, which are assigned to the following transitions:
9 $^2\text{H}_{9/2}-^4\text{I}_{15/2}$ (409 nm), $^2\text{H}_{11/2}-^4\text{I}_{15/2}$ (524 nm), $^4\text{S}_{3/2}-^4\text{I}_{15/2}$ (549 nm), and $^4\text{F}_{9/2}-^4\text{I}_{15/2}$ (670 nm). The spectral line
10 positions of $\text{La}_2\text{O}_2\text{S}:\text{Er}^{3+}$ spectra are the same. Change of host leads to the intensity redistribution, which is
11 most pronounced for $^4\text{I}_{15/2}-^4\text{G}_{11/2}$ transition in the excitation spectrum.

12 Fig. 6 displays excitation and emission spectra of $\text{RE}_2\text{O}_2\text{S}$ (RE = Y, La) activated by 1% of Eu^{3+} ions. The
13 excitation spectrum of $\text{Y}_2\text{O}_2\text{S}:\text{Eu}^{3+}$ monitored at 545 nm ($^5\text{D}_1-^7\text{F}_1$) consists of following transitions: $^7\text{F}_0-^5\text{D}_4$
14 (353 nm), $^7\text{F}_0-^5\text{L}_7$ (378 nm) and $^7\text{F}_2-^5\text{D}_2$ (488 nm). The emission spectrum shows narrow bands originating
15 from $^5\text{D}_1$ and $^5\text{D}_0$ excited levels. Surprisingly, that the emission spectrum of $\text{Y}_2\text{O}_2\text{S}:\text{Eu}^{3+}$ is dominated by
16 transition $^5\text{D}_1-^7\text{F}_1$ (545 nm), whereas the most prominent luminescence bands are usually attributed to the
17 $^5\text{D}_0-^7\text{F}_j$ transition [46–48]. Such behavior was previously reported for $\text{La}_2\text{O}_2\text{S}:\text{Eu}^{3+}$ bulk phosphors [49, 50].
18 Dominance of $^5\text{D}_1$ emission can be explained by small phonon energy in regarded host, because significant
19 amount of ions relax to $^5\text{D}_1$ level after the UV excitation, and they radiatively decay to the ground state
20 before nonradiative decay to $^5\text{D}_0$ metastable level. We also observed $^5\text{D}_2-^7\text{F}_2$ (490 nm), $^5\text{D}_1-^7\text{F}_3$ (587 nm),
21 $^5\text{D}_0-^7\text{F}_1$ (592 nm), $^5\text{D}_0-^7\text{F}_2$ (621 nm) and $^5\text{D}_0-^7\text{F}_3$ (670 nm) transitions.

22 The excitation and emission spectra of $\text{La}_2\text{O}_2\text{S}:\text{Eu}^{3+}$ display situation, which is more usual for Eu^{3+} -doped
23 compounds. The excitation spectrum of $\text{Y}_2\text{O}_2\text{S}:\text{Eu}^{3+}$ monitored at 623 nm ($^5\text{D}_0-^7\text{F}_2$) consists of broad
24 intense band corresponding to charge transfer $\text{S}^{2-}-\text{Eu}^{3+}$ (338 nm) and low-intense line assigned to the typical
25 intra-configurational transitions of the Eu^{3+} ion: $^7\text{F}_0-^5\text{L}_6$ (394 nm), $^7\text{F}_0-^5\text{D}_2$ (466 nm), $^7\text{F}_0-^5\text{D}_1$ (536 nm) and
26 $^7\text{F}_1-^5\text{D}_0$ (593 nm). The emission spectrum is dominated by the forced electric dipole transition $^5\text{D}_0-^7\text{F}_2$ with
27 maximum at 623 nm. Other observed lines are attributed to the $^5\text{D}_1-^7\text{F}_1$ (538 nm), $^5\text{D}_1-^7\text{F}_2$ (555 nm), $^5\text{D}_1-^7\text{F}_3$
28 (586 nm), $^5\text{D}_0-^7\text{F}_1$ (594 nm), $^5\text{D}_0-^7\text{F}_3$ (670 nm) and $^5\text{D}_0-^7\text{F}_4$ (704 nm).

29 Due to the unique luminescence properties of Eu^{3+} ions, it is quite easy to analyze the luminescent center
30 local surrounding and its symmetry using only emission spectrum. The asymmetry ratio (R_{Eu}) gives
31 information about local changes around the Eu^{3+} ions. It is defined as intensity ratio of forced electric dipole
32 $^5\text{D}_0-^7\text{F}_2$ and magnetic dipole $^5\text{D}_0-^7\text{F}_1$ transitions. The higher the asymmetry parameter R_{Eu} is, the more apart
33 from a centrosymmetric geometry luminescent center is located. The calculated R_{Eu} values of $\text{Y}_2\text{O}_2\text{S}:\text{Eu}^{3+}$
34 and $\text{La}_2\text{O}_2\text{S}:\text{Eu}^{3+}$ samples are 0.58 and 3.16, respectively. It is worth noting that the calculated R_{Eu} values of
35 $\text{Y}_2\text{O}_2\text{S}:\text{Eu}^{3+}$ and $\text{La}_2\text{O}_2\text{S}:\text{Eu}^{3+}$ samples significantly differ, which indicate big difference in local surrounding
36 of Eu^{3+} ions in these hosts.

37 The steady state luminescence spectra of $\text{RE}_2\text{O}_2\text{S}$ (RE = Y, La) powders doped with 1% of Ce^{3+} ions are
38 shown in Fig. 7. The excitation spectrum of $\text{Y}_2\text{O}_2\text{S}:\text{Ce}^{3+}$ sample displays two broad bands centered at 265
39 and 407 nm ($\lambda_{em} = 545$ nm). These bands correspond to direct excitation of the Ce^{3+} ions via transitions to
40 the components of Ce^{3+} 5d configuration. The emission spectrum also consists of two lines attributed to
41 allowed 5d–4f transition of Ce^{3+} ion. Generally, emission lines attributed to allowed 5d–4f transition in
42 Ce^{3+} -doped materials are quite broad [51, 52]. Sometimes they are split into two components separated by
43 approximately 2000 cm^{-1} due to the spin-orbit splitting of the $4f^1$ ground state into two components $^2\text{F}_{5/2}$ and
44 $^2\text{F}_{7/2}$. The bands observed in $\text{Y}_2\text{O}_2\text{S}:\text{Ce}^{3+}$ and $\text{La}_2\text{O}_2\text{S}:\text{Ce}^{3+}$ exhibit splitting by 5000 cm^{-1} and cannot be due
45 to splitting of the ground state mentioned above. Therefore, two bands in Ce^{3+} luminescence must be
46 ascribed to the electron transitions from the lowest and second 5d levels to the ground state of Ce^{3+} [53].

1 Change of host to La₂O₂S does not affect spectroscopic properties of Ce³⁺-doped material. The line positions
2 are almost the same for both excitation and emission spectra.

4. Conclusions

3
4
5 In summary, a method for the production of luminescent materials on the basis of rare-earth oxysulfides was
6 developed. The advantage of the method consists in the precipitation of a sulfur-containing precursor from a
7 homogeneous nitrate solution and subsequent transformation in a reducing and sulfidating atmosphere. The
8 use of chemical homogenization made it possible to achieve an excellent uniform distribution of cations in
9 the structure. The use of sulfates as precursors, in view of the presence of sulfur in the structure, greatly
10 simplifies the process of obtaining solid solutions of oxysulfides. All synthesized samples have single phase
11 without any impurities. The excitation and emission spectra of RE₂O₂S:Ln (RE = Y, La; Ln = Dy, Er, Eu)
12 consist of characteristic bands corresponding to the 4f-4f intra configurational transitions. The study of Dy³⁺
13 and Eu³⁺-doped powders revealed that Y₂O₂S host possesses higher local symmetry than La₂O₂S one. The
14 excitation and emission spectra of RE₂O₂S:Ce³⁺ (RE = Y, La) phosphor displayed allowed 5d-4f transition.

Acknowledgement

15
16
17
18 The authors would like to thank the staff of the Engineering Center of the Tyumen State University for their
19 help in carrying out physical and chemical tests. We also thank Andrey Bobylev for conducting electron
20 microscopy.

References

- 21
22
23 [1] Yu.G. Denisenko, A.S. Aleksandrovsky, V.V. Atuchin, A.S. Krylov, M.S. Molokeev, A.S. Oreshonkov,
24 N.P. Shestakov, O.V. Andreev, Exploration of structural, thermal and spectroscopic properties of self-
25 activated sulfate Eu₂(SO₄)₃ with isolated SO₄ groups, *J. Ind. Eng. Chem.* 68 (2018) 109-116.
26 <https://doi.org/10.1016/j.jiec.2018.07.034>
27 [2] Y.G. Denisenko, V.V. Atuchin, M.S. Molokeev, A.S. Aleksandrovsky, A.S. Krylov, A.S.
28 Oreshonkov, S. S. Volkova, O.V. Andreev, Structure, thermal stability, and spectroscopic properties of
29 triclinic double sulfate AgEu(SO₄)₂ with Isolated SO₄ Groups, *Inorg. Chem.*, 57 (21) (2018) 13279-13288.
30 <https://doi.org/10.1021/acs.inorgchem.8b01837>
31 [3] X. Shi, Z. Wang, T. Takei, X. Wang, Q. Zhu, X. Li, B.-N. Kim, X. Sun, J.-G. Li, Selective
32 Crystallization of Four Tungstates (La₂W₃O₁₂, La₂W₂O₉, La₁₄W₈O₄₅, and La₆W₂O₁₅) via Hydrothermal
33 Reaction and Comparative Study of Eu³⁺ Luminescence, *Inorg. Chem.* 57 (11) (2018) 6632-6640.
34 <https://doi.org/10.1021/acs.inorgchem.8b00807>
35 [4] F. Baur, T. Jüstel, Uranyl sensitized Eu³⁺ luminescence in Ln(UO₂)₃(PO₄)₂ O(OH)·6H₂O phosphors (Ln
36 = Y, Eu, La) for warm-white light emitting diodes, *J. Lum.* 196 (2018) 431-436.
37 <https://doi.org/10.1016/j.jlumin.2017.12.073>
38 [5] V.V. Atuchin, A.S. Aleksandrovsky, O.D. Chimitova, T.A. Gavrilova, A.S. Krylov, M.S.
39 Molokeev, A.S. Oreshonkov, B.G. Bazarov, J.G. Bazarova, Synthesis and spectroscopic properties of
40 monoclinic α-Eu₂(MoO₄)₃, *J. Phys. Chem. C.* 118 (28) (2014), 15404-15411.
41 <https://org/doi/10.1021/jp5040739>
42 [6] V.V. Atuchin, A.K. Subanakov, A.S. Aleksandrovsky, B.G. Bazarov, J.G. Bazarova, T.A. Gavrilova,
43 A.S. Krulov, M.S. Molokeev, A.S. Oreshonkov, S.Yu. Stefanovich, Structural and spectroscopic properties
44 of noncentrosymmetric self-activated borate Rb₃EuB₆O₁₂ with B₅O₁₀ units, *Mater. Des.* 140 (2018) 488-494.
45 <https://doi.org/10.1016/j.matdes.2017.12.004>

- [7] J. Lian, F. Liu, J. Zhang, Y. Yang, X. Wang, Z. Zhang, F. Liu, Template-free hydrothermal synthesis of $\text{Gd}_2\text{O}_2\text{SO}_4:\text{Eu}^{3+}$ hollow spheres based on urea-ammonium sulfate (UAS) system, *Optik*. 127 (20) (2016) 8621-8628. <https://doi.org/10.1016/j.ijleo.2016.06.069>
- [8] J. Lian, F. Liu, X. Wang, X. Sun, Hydrothermal synthesis and photoluminescence properties of $\text{Gd}_2\text{O}_2\text{SO}_4:\text{Eu}^{3+}$ spherical phosphor, *Powder Tech.* 253. (2014) 187-192. <https://doi.org/10.1016/j.powtec.2013.11.021>
- [9] Li X., Lian J. Synthesis and characterizations of pompon-like $\text{Y}_2\text{O}_2\text{SO}_4:\text{Eu}^{3+}$ phosphors using a UBHP technique based on UAS system, *Optik*. 127 (1) (2016) 401-406. <https://doi.org/10.1016/j.ijleo.2015.10.091>
- [10] J. Lian, H. Qin, P. Liang, F. Liu, Co-precipitation synthesis of $\text{Y}_2\text{O}_2\text{SO}_4:\text{Eu}^{3+}$ nanophosphor and comparison of photoluminescence properties with $\text{Y}_2\text{O}_3:\text{Eu}^{3+}$ and $\text{Y}_2\text{O}_2\text{S}:\text{Eu}^{3+}$ nanophosphors, *Solid State Sci.* 48 (2015) 147-154. <https://doi.org/10.1016/j.solidstatesciences.2015.08.004>
- [11] H. Jiao, Y. Wang, $\text{Ca}_2\text{Al}_2\text{Si}_2\text{O}_7:\text{Ce}^{3+}, \text{Tb}^{3+}$: A white-light phosphor suitable for whitelight-emitting diodes, *J. Electrochem. Society*, 156 (2009) J117–J120. <http://jes.ecsdl.org/content/156/5/J117.short>
- [12] R. Shrivastava, J. Kaur, V. Dubey, White light emission by Dy^{3+} doped phosphor matrices: A short review, *J. of Fluorescence*. 26 (1) (2016) 105 – 111. <https://doi.org/10.1007/s1089>
- [13] F. Yang, H. Ma, Y. Liu, B. Han, H. Feng, Q. Yu, Photoluminescence properties of novel Dy^{3+} doped $\text{Ba}_5\text{GaAl}_4\text{O}_{12}$ phosphors, *Ceram. Int.* 40 (2014) 10189 – 10192. <https://doi.org/10.1016/j.ceramint.2014.02.068>
- [14] B. M. Cheng, C.K. Duan, P.A. Tanner, Vacuum ultraviolet and visible spectra of Eu^{3+} in $\text{Y}_2\text{O}_2\text{S}$ and $\text{Eu}_2\text{O}_2\text{S}$, *Opt. Mat.* 31 (6) (2009) 902 - 904. <https://doi.org/10.1016/j.optmat.2008.10.036>
- [15] J. Thirumalai, R. Chandramohan, S. Valanarasu, T. A. Vijayan, R. M. Somasundaram, T. Mahalingam, S. R. Srikumar, Shape-selective synthesis and opto-electronic properties of Eu^{3+} -doped gadolinium oxysulfide nanostructures, *J. Mater. Sci.* 44 (14) (2009) 3889-3899. <https://doi.org/10.1007/s10853-009-3531-7>
- [16] X. Lu, L. Yang, Q. Ma, J. Tian, X. Dong, A novel strategy to synthesize $\text{Gd}_2\text{O}_2\text{S}:\text{Eu}^{3+}$ luminescent nanobelts via inheriting the morphology of precursor, *J. Mater. Sci.: Mater. in Electronics*. 25 (12) (2014) 5388-5394. <https://doi.org/10.1007/s10854-014-2317-0>
- [17] S.A. Osseni, S. Lechevallier, M. Verelst, C. Dujardin, J. Dexpert-Ghys, D. Neumeyer, M. Leclercq, H. Baaziz, D. Cussac, V. Santran, R. Mauricot, New nanoplatform based on $\text{Gd}_2\text{O}_2\text{S}:\text{Eu}^{3+}$ core: synthesis, characterization and use for in vitro bio-labelling, *J. Mater. Chem.* 21 (45) (2011) 18365-18372. <https://doi.org/10.1039/C1JM13542B>
- [18] S.A. Osseni, S. Lechevallier, M. Verelst, P. Perriat, J. Dexpert-Ghys, D. Neumeyer, R. Garcia, F. Maye^d, K. Djanashvili, J.A. Peters, E. Magdeleine, H. Gros-Dagnac, P. Celsis, R. Mauricot, Gadolinium oxysulfide nanoparticles as multimodal imaging agents for T 2-weighted MR, X-ray tomography and photoluminescence, *Nanoscale*. 6 (1) (2014) 555-564. <https://doi.org/10.1039/C3NR03982J>
- [19] Q. Zhao, Y. Zheng, N. Guo, Y. Jia, H. Qiao, W. Lv, H. You, 3D-hierarchical $\text{Lu}_2\text{O}_2\text{S}:\text{Eu}^{3+}$ micro/nanostructures: controlled synthesis and luminescence properties, *CrystEngComm*. 14 (20) (2012) 6659-6664. <https://doi.org/10.1039/C2CE25631B>
- [20] Y. Yang, C. Mi, F. Yu, X. Su, C. Guo, G. Li, J. Zhang, L. Liu, Y. Liu, X. Li, Optical thermometry based on the upconversion fluorescence from $\text{Yb}^{3+}/\text{Er}^{3+}$ codoped $\text{La}_2\text{O}_2\text{S}$ phosphor, *Ceram. Int.* 40 (7 Part A) (2014) 9875-9880. <https://doi.org/10.1016/j.ceramint.2014.02.081>
- [21] S. Yokono, T. Abe, T. Hoshina, Red luminescence of Ce^{3+} to the large stokes shifts in $\text{Y}_2\text{O}_2\text{S}$ and $\text{Lu}_2\text{O}_2\text{S}$, *J. Lum.* 24/25 (Part 1) (1981) 309-312. [https://doi.org/10.1016/0022-2313\(81\)90279-9](https://doi.org/10.1016/0022-2313(81)90279-9)
- [22] Y. Yang, C. Mi, F. Yu, X. Su, C. Guo, G. Li, J. Zhang, L. Liu, Y. Liu, X. Li, Optical thermometry based on the upconversion fluorescence from $\text{Yb}^{3+}/\text{Er}^{3+}$ codoped $\text{La}_2\text{O}_2\text{S}$ phosphor // *Ceram. Int.* 2014. V. 40. № 7, Part A. P. 9875-9880. <https://doi.org/10.1016/j.ceramint.2014.02.081>

- [23] X. Wang, Z. Zhang, Z. Tang, Y. Lin, Characterization and properties of a red and orange Y_2O_2S -based long afterglow phosphor, *Mater. Chem. Phys.* 80 (2003) 1-5. [https://doi.org/10.1016/S0254-0584\(02\)00097-4](https://doi.org/10.1016/S0254-0584(02)00097-4)
- [24] G.A. Kumar, M. Pokhrel, A. Martinez, R.C. Dennis, I.L. Villegas, D.K. Sardar, Synthesis and spectroscopy of color tunable $Y_2O_2S:Yb^{3+}, Er^{3+}$ phosphors with intense emission, *J. Alloy. Compd.* 513 (2012) 559 – 565. <https://doi.org/10.1016/j.jallcom.2011.11.006>
- [25] T.W. Chou, S. Mylswamy, R.S. Liu, S.Z. Chuang, Eu substitution and particle size control of Y_2O_2S for the excitation by UV light emitting diodes, *Solid State Comm.* 136 (2005) 205 – 209. <https://doi.org/10.1016/j.ssc.2005.07.032>
- [26] H. Wang, M. Xing, X. Luo, X. Zhou, Y. Fu, T. Jiang, Y. Peng, Y. Ma, X. Duan, Up-conversion emission colour modulation of $Y_2O_2S:Yb, Er$ under 1.55 μm and 980 nm excitation, *J. Alloy. Compd.* 587 (2014) 344 – 348. <https://doi.org/10.1016/j.jallcom.2013.10.163>
- [27] Yu.G. Denisenko, N.A. Khritokhin, O.V. Andreev, S.A. Basova, E.I. Sal'nikova, A.A. Polkovnikov, Thermal decomposition of europium sulfates $Eu_2(SO_4)_3 \cdot 8H_2O$ and $EuSO_4$, *J. Solid State Chem.* 255 (2017) 219 – 224. <https://doi.org/10.1016/j.jssc.2017.08.020>
- [28] H. Stark, R.L.N. Yatavelli, S. L. Thompson, H. Kang, J. E. Krechmer, J. R. Kimmel, B.B. Palm, W. Hu, P.L. Hayes, D.A. Day, P. Campuzano-Jost, M.R. Canagaratna, J.T. Jayne, D.R. Worsnop, J.L. Jimenez, Impact of thermal decomposition on thermal desorption instruments: advantage of thermogram analysis for quantifying volatility distributions of organic species, *Environ. Sci. Technol.* 51 (15) (2017) 8491–8500. <https://doi.org/10.1021/acs.est.7b00160>
- [29] O.V. Andreev, I.A. Razumkova, A.N. Boiko. Synthesis and thermal stability of rare earth compounds RE_3F_3 , $RE_3F_3 \cdot nH_2O$ and $(H_3O)RE_3F_{10} \cdot nH_2O$ ($RE = Tb - Lu, Y$), obtained from sulfide precursors, *J. Fluor. Chem.* 207(2018)77-83. <https://doi.org/10.1016/j.jfluchem.2017.12.001>
- [30] I.A. Razumkova, Synthesis of $NaYF_4$ compounds from sulfide precursors, *J. Fluor. Chem.* 205(2018) 1-4. <https://doi.org/10.1016/j.jfluchem.2017.10.012>
- [31] M. Unni, A.M. Uhl, S. Savliwala, B.H. Savitzky, R. Dhavalikar, N. Garraud, D.P. Arnold, L.F. Kourkoutis, J.S. Andrew, C. Rinaldi, Thermal decomposition synthesis of iron oxide nanoparticles with diminished magnetic dead layer by controlled addition of oxygen, *ACS Nano.* 11 (2) (2017) 2284 – 2303. <https://doi.org/10.1021/acs.nano.7b00609>
- [32] S.A. Osseni, Yu.G. Denisenko, J.K. Fatombi, E.I. Sal'nikova, O.V. Andreev, Synthesis and characterization of $Ln_2O_2SO_4$ ($Ln = Gd, Ho, Dy$ and Lu) nanoparticles obtained by coprecipitation method and study of their reduction reaction under H_2 flow, *J. Nanostr. Chem.* 7 (4) (2017) 337 – 343. <https://doi.org/10.1007/s40097-017-0243-4>
- [33] P.O. Andreev, E.I. Sal'nikova, O.V. Andreev, Yu.G. Denisenko, I.M. Kovenskii, Synthesis and Upconversion Luminescence Spectra of $(Y_{1-x-y}Yb_xEr_y)_2O_2S$, *Inorg. Mater.* 53 (2) (2017) 200 – 206. <https://doi.org/10.1134/S0020168517020029>
- [34] P.O. Andreev, E.I. Sal'nikova, I.M. Kovenski, Preparation of Ln_2O_2S ($Ln = Gd, Dy, Y, Er, Lu$) in flowing hydrogen and hydrogen sulfide, *Inorg. Mater.* 50 (2014) 1018 – 1023. <https://doi.org/10.1134/S0020168517020029>
- [35] O.V. Andreev, Yu.G. Denisenko, E.I. Sal'nikova, N.A. Khritokhin, K.S. Zyryanova, Specifics of Reactions of Cerium Sulfate and Europium Sulfate with Hydrogen, *Russ. J. Inorg. Chem.* 61 (2016) 296 – 301. <https://doi.org/10.1134/S0036023616030025>
- [36] P.O. Andreev, E.I. Sal'nikova, O.V. Andreev, I.M. Kovenskii, Kinetic Schemes of Chemical Transformations and Particle Morphology upon Interaction between $Ln_2(SO_4)_3$ ($Ln = La, Pr, Nd, Sm$) and Hydrogen // *Russ. J. Phys. Chem. A.* 90 (1) (2016) 25 –30. <https://doi.org/10.1134/S0036024416010027>

- [37] E.I. Sal'nikova, P.O. Andreev, S.M. Antonov, Kinetic Diagrams of $\text{Ln}_2\text{O}_2\text{SO}_4$ Phase Transformations in a H_2 Flow ($\text{Ln} = \text{La}, \text{Pr}, \text{Nd}, \text{Sm}$), *Russ. J. Phys. Chem. A.* 87 (8) (2013) 1280 – 1283.
<https://doi.org/10.1134/S0036024413080207>
- [38] P.O. Andreev, E.I. Sal'nikova, A.A. Kislytsyn, Kinetics of the transformation of $\text{Ln}_2\text{O}_2\text{SO}_4$ into $\text{Ln}_2\text{O}_2\text{S}$ ($\text{Ln} = \text{La}, \text{Pr}, \text{Nd}, \text{Sm}$) in a hydrogen flow, *Russ. J. Phys. Chem. A.* 87 (9) (2013) 1482 – 1487.
<https://doi.org/10.1134/S0036024413080050>
39. Bruker AXS TOPAS V4: General profile and structure analysis software for powder diffraction data. User's Manual. Bruker AXS, Karlsruhe, Germany. 2008.
- [40] J. Kuang, Y. Liu, J. Zhang, White-light-emitting long-lasting phosphorescence in Dy^{3+} -doped SrSiO_3 , *J. Solid State Chem.* 179 (2006) 266 – 269. <https://doi.org/10.1016/j.jssc.2005.10.025>
- [41] P. Babu, K.H. Jang, E.S. Kim, L. Shi, H.J. Seo, F. Rivera-López, U.R. Rodriguez-Mendoza, V. Lavin, R. Vijaya, C.K. Jayasankar L.R. Moorthy, Spectral investigations on Dy^{3+} -doped transparent oxyfluoride glasses and nanocrystalline glass ceramics, *J. Appl. Phys.* 105 (2009) 13516.
<https://doi.org/10.1063/1.3021451>
- [42] I.E. Kolesnikov, A.A. Kalinichev, M.A. Kurochkin, E.V. Golyeva, A.S. Terentyeva, E.Yu. Kolesnikov, E. Lähderanta, Structural, luminescence and thermometric properties of nanocrystalline YVO_4 : Dy^{3+} temperature and concentration series, *Sci. reports.* 9 (1) (2019) 2043. <https://doi.org/10.1038/s41598-019-38774-6>
- [43] I.E. Kolesnikov, A.V. Povolotskiy, D.V. Mamonova, E.Y. Kolesnikov, A.V. Kurochkin, E. Lähderanta, M.D. Mikhailov, Asymmetry ratio as a parameter of Eu^{3+} local environment in phosphors, *J. Rare Earths.* 36 (2018) 474 – 481. <https://doi.org/10.1016/j.jre.2017.11.008>
- [44] E. Oomen, A.-M.A. Van Dongen, Europium (III) in oxide glasses: dependence of the emission spectrum upon glass composition, *J. Non. Cryst. Solids.* 111 (1989) 205-213. [https://doi.org/10.1016/0022-3093\(89\)90282-2](https://doi.org/10.1016/0022-3093(89)90282-2)
- [45] U. Fawad, H.J. Kim, S. Khan, M. Khan, L. Ali, Photoluminescent properties of white-light-emitting $\text{Li}_6\text{Y}(\text{BO}_3)_3:\text{Dy}^{3+}$ phosphor, *Solid State Sci.* 62 (2016) 1–5.
<https://doi.org/10.1016/j.solidstatesciences.2016.08.008>
- [46] Y.A. Dolinskaya, I.E. Kolesnikov, A.V. Kurochkin, A.A. Man'shina, M.D. Mikhailov, and A.V. Semench, Sol-gel synthesis and luminescent properties of $\text{YVO}_4:\text{Eu}$ nanoparticles, *Glass Phys. Chem.* 39 (3) (2013) 308 – 310. <https://doi.org/10.1134/S1087659613030061>
- [47] I.E. Kolesnikov, A.V. Povolotskiy, D.V. Tolstikova, A.A. Manshina, M.D. Mikhailov, Luminescence of $\text{Y}_3\text{Al}_5\text{O}_{12}:\text{Eu}^{3+}$ nanophosphors in blood and organic media, *J. Phys. D.* 48 (7) (2015) 075401. <https://doi.org/10.1088/0022-3727/48/7/075401/meta>
- [48] I.E. Kolesnikov, D.V. Mamonova, E. Lähderanta, A.V. Kurochkin, M.D. Mikhailov, The impact of doping concentration on structure and photoluminescence of $\text{Lu}_2\text{O}_3:\text{Eu}^{3+}$ nanocrystals, *J. Lum.* 187 (2017) 26 – 32. <https://doi.org/10.1016/j.jlumin.2017.03.006>
- [49] Q. Dai, H. Song, M. Wang, X. Bai, B. Dong, R. Qin, X. Qu, H. Zhang, Size and Concentration Effects on the Photoluminescence of $\text{La}_2\text{O}_2\text{S}:\text{Eu}^{3+}$ Nanocrystals, *J. Phys. Chem. C.* 112 (49) (2008) 19399-19404. <https://doi.org/10.1021/jp808343f>
- [50] R.H. Krauss, R.G. Hellier, J.C. McDaniel, Surface temperature imaging below 300 K using $\text{La}_2\text{O}_2\text{S}:\text{Eu}$, *Appl. Opt.* 33 (18) (1994) P. 3901 – 3904. <https://doi.org/10.1364/AO.33.003901>
- [51] M. Upasani, B. Butey, S.V. Moharil, Synthesis, characterization and optical properties of $\text{Y}_3\text{Al}_5\text{O}_{12}:\text{Ce}$ phosphor by mixed fuel combustion synthesis, *J. Alloy. Compd.* 650 (2015) 858 – 862.
<https://doi.org/10.1016/j.jallcom.2015.08.076>

- 1 [52] H.-L. Li, X.-J. Liu, L.-P. Huang, Luminescent properties of LuAG:Ce phosphors with different Ce
2 contents prepared by a sol-gel combustion method, *Opt. Mater. (Amst)*. 29 (2007) 1138–1142.
3 <https://doi.org/10.1016/j.optmat.2006.05.002>
4 [53] J.-J. Zhao, C.-X. Guo, R.-W. Guo, J.-T. Hu, Red luminescence of $\text{Lu}_2\text{O}_2\text{S}:\text{Ce}$ and $\text{Y}_2\text{O}_2\text{S}:\text{Ce}$ at room
5 temperature, *J. Alloy. Compd.* 436 (2007) 174–177. <https://doi.org/10.1016/j.jallcom.2006.06.103>
6
7

8 Captions

9 Fig.1. Experimental, calculated, and difference Rietveld plot of: a,b) $(\text{RE}_{0.99}\text{Ln}_{0.01})_2(\text{SO}_4)_3$; c,d)
10 $(\text{RE}_{0.99}\text{Ln}_{0.01})_2(\text{SO}_4)_3-(\text{RE}_{0.99}\text{Ln}_{0.01})_2\text{O}_2\text{SO}_4-(\text{RE}_{0.99}\text{Ln}_{0.01})_2\text{O}_2\text{S}-(\text{RE}_{0.99}\text{Ln}_{0.01})_2\text{O}_3$; e,f) $(\text{RE}_{0.99}\text{Ln}_{0.01})_2\text{O}_2\text{S} -$
11 $(\text{RE}_{0.99}\text{Ln}_{0.01})_2\text{O}_3$; g,h) $(\text{RE}_{0.99}\text{Ln}_{0.01})_2\text{O}_2\text{S}$.

12 Fig. 2. SEM image of a) $(\text{La}_{0.99}\text{Dy}_{0.01})_2(\text{SO}_4)_3$; b) $(\text{La}_{0.99}\text{Dy}_{0.01})_2\text{O}_2\text{S}$

13 Fig. 3. Coordination polyhedron structure $\text{La}_2\text{O}_2\text{S}$

14 Fig. 4. Excitation and emission spectra of $\text{Y}_2\text{O}_2\text{S}:\text{Dy}^{3+}$ and $\text{La}_2\text{O}_2\text{S}:\text{Dy}^{3+}$ phosphors

15 Fig. 5. Excitation and emission spectra of $\text{Y}_2\text{O}_2\text{S}:\text{Er}^{3+}$ and $\text{La}_2\text{O}_2\text{S}:\text{Er}^{3+}$ phosphors

16 Fig. 6. Excitation and emission spectra of $\text{Y}_2\text{O}_2\text{S}:\text{Eu}^{3+}$ and $\text{La}_2\text{O}_2\text{S}:\text{Eu}^{3+}$ phosphors

17 Fig. 7. Excitation and emission spectra of $\text{Y}_2\text{O}_2\text{S}:\text{Ce}^{3+}$ and $\text{La}_2\text{O}_2\text{S}:\text{Ce}^{3+}$ phosphors

1
2
3

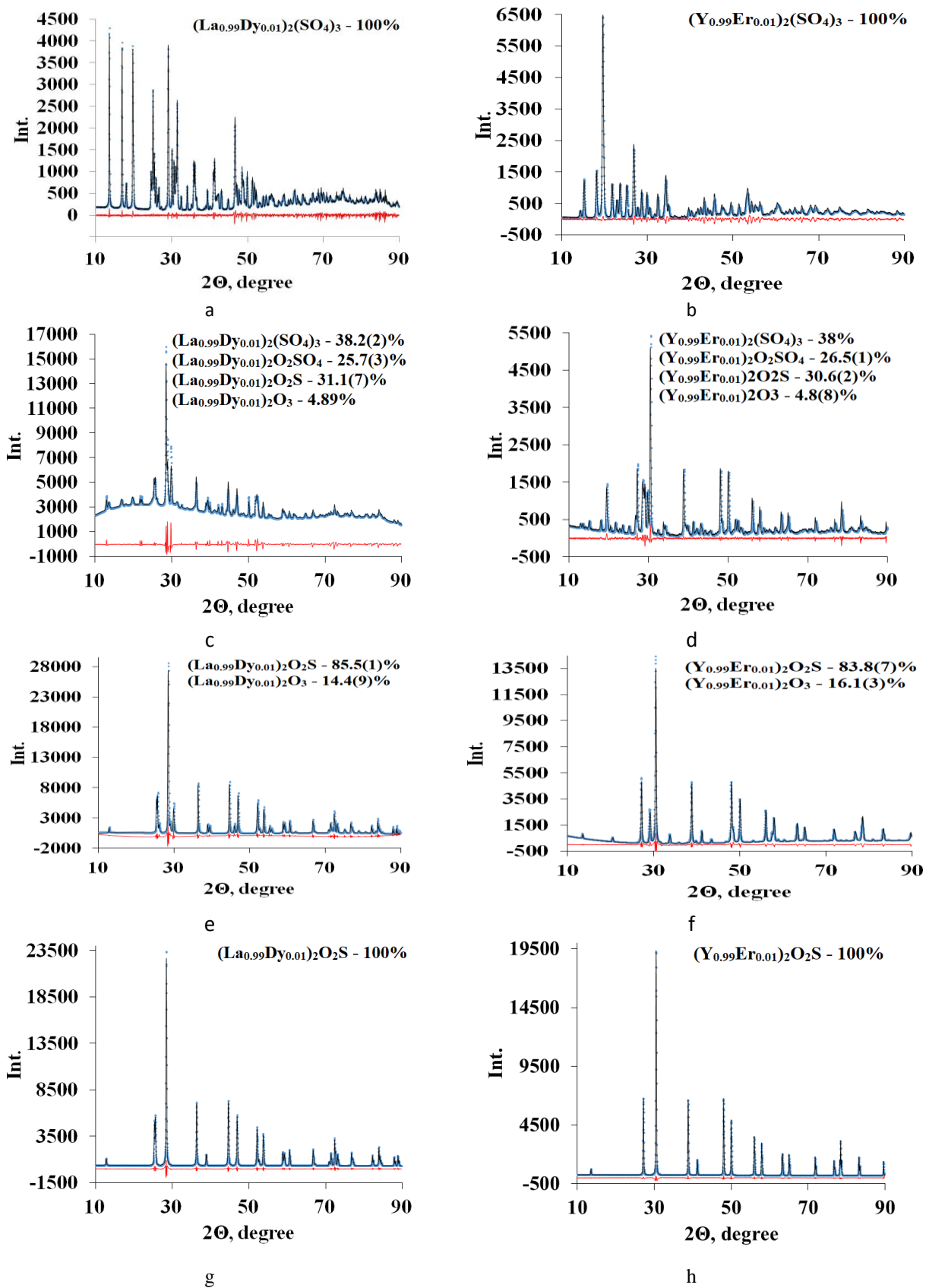
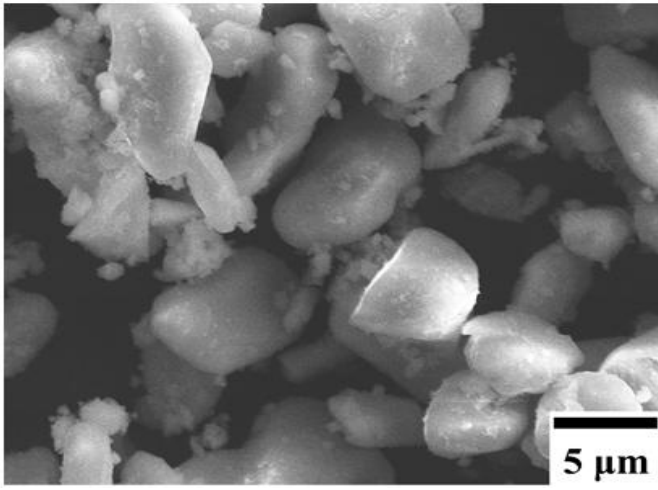
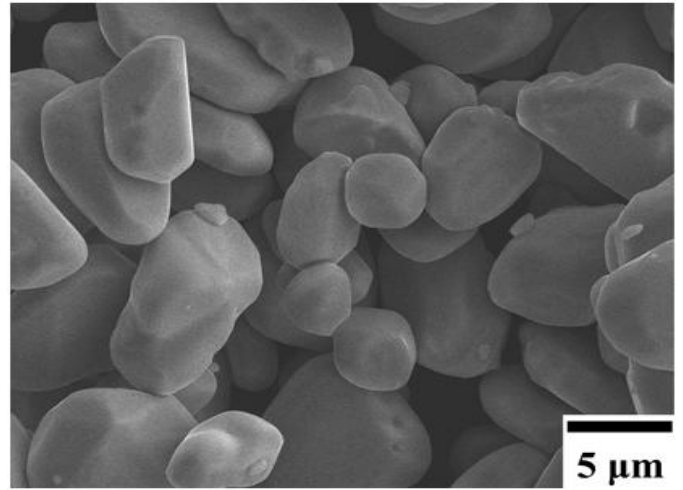


Fig. 1

4



a)



b)

Fig. 2

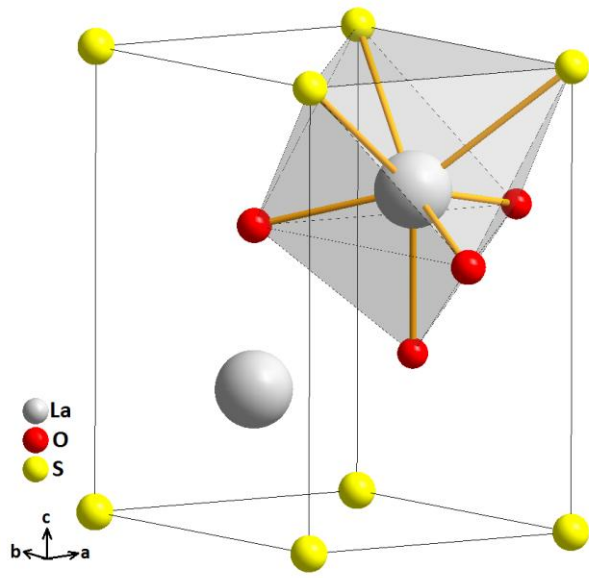


Fig. 3.

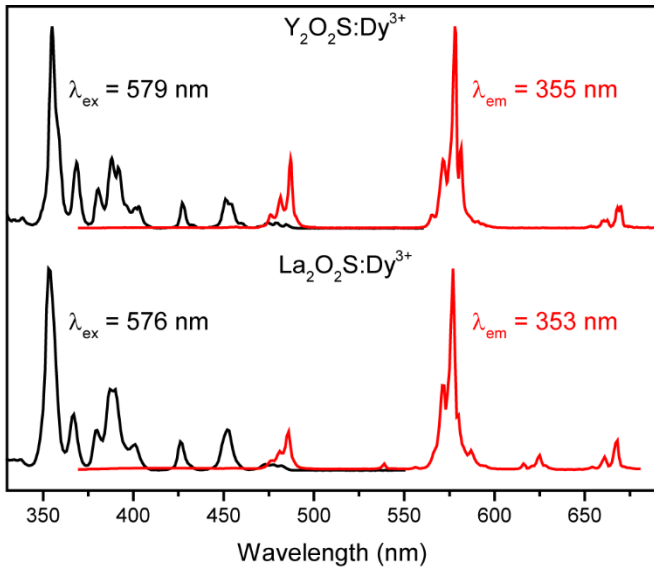


Fig. 4

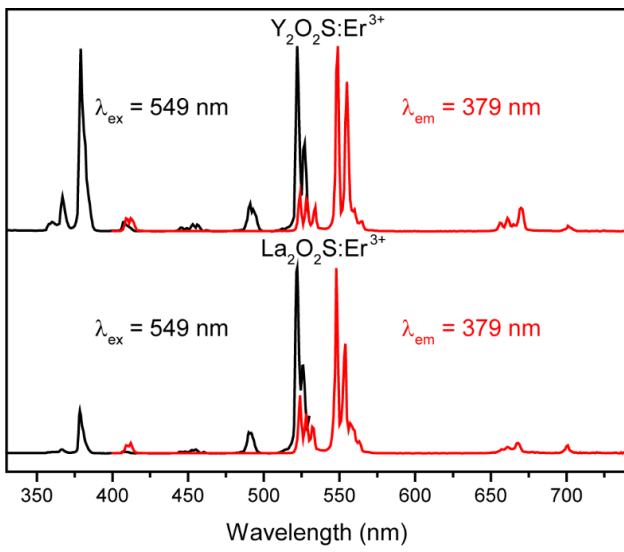


Fig. 5

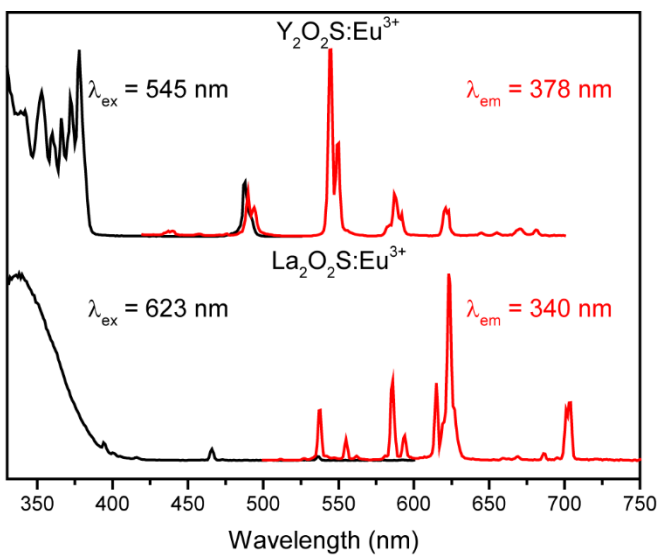
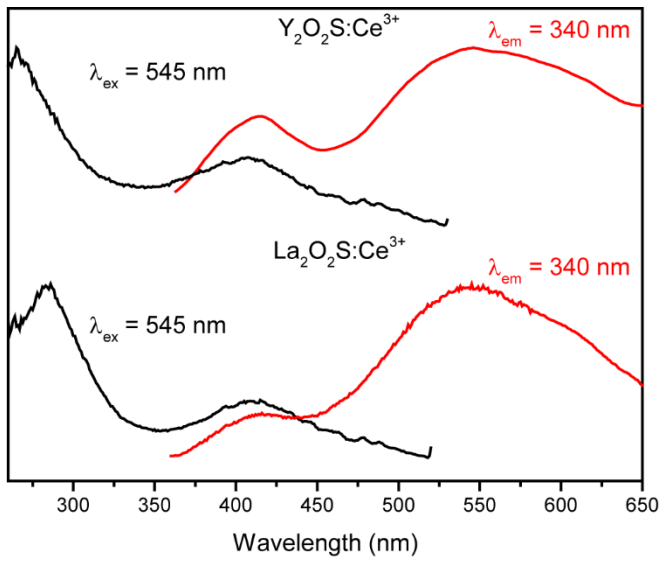


Fig. 6



1
2 Fig. 7

Table 1. Main parameters of processing and refinement of the samples La-O-S

Compound	Phase	Weight (%)	Space group	Cell parametrs ($^{\circ}$, \AA), Cell volume (\AA^3)	R_{wp} , R_p (%)	X^2
$(La_{0.99}Dy_{0.01})_2(SO_4)_3$	$(La_{0.99}Dy_{0.01})_2(SO_4)_3$	100	$C2/c$	a=22.1136 b=6.9036 c=7.1198 V=1035.15(3)	6.34 4.77	1.51
$(La_{0.99}Dy_{0.01})_2(SO_4)_3$ - $(La_{0.99}Dy_{0.01})_2O_2SO_4$ - $(La_{0.99}Dy_{0.01})_2O_2S$ - $(La_{0.99}Dy_{0.01})_2O_3$	$(La_{0.99}Dy_{0.01})_2(SO_4)_3$	38.2(2)	$C2/c$	a=22.1138 b=6.9026 c=7.1204 V=1035.18(1)	5.31 4.35	7.72
	$(La_{0.99}Dy_{0.01})_2O_2SO_4$	25.7(3)	$C2/c$	a=14.3493 b=4.2858 c=8.3882 V=493.43(1)		
	$(La_{0.99}Dy_{0.01})_2O_2S$	31.1(7)	$P-3m 1$	a=4.0520 c=6.9420 V=98.70(8)		
	$(La_{0.99}Dy_{0.01})_2O_3$	4.7(9)	$P-3m 1$	a=4.0520 c=6.9420 V=82.67(0)		
$(La_{0.99}Dy_{0.01})_2O_2S$ - $(La_{0.99}Dy_{0.01})_2O_3$	$(La_{0.99}Dy_{0.01})_2O_2S$	85.5(1)	$P-3m 1$	a=4.0521 c=6.9428 V=98.72(5)	12.97 9.91	9.12
	$(La_{0.99}Dy_{0.01})_2O_3$	14.4(9)	$P-3m 1$	a=3.9402 c=6.1493 V=82.67(9)		
$(La_{0.99}Dy_{0.01})_2O_2S$	$(La_{0.99}Dy_{0.01})_2O_2S$	100	$P-3m 1$	a=4.0520 c=6.9425 V=98.71(6)	4.71 3.51	1.46

Table 2. Main parameters of processing and refinement of the samples Y-O-S

Compound	Phase	Weight (%)	Space group	Cell parametrs ($^{\circ}$, \AA), Cell volume (\AA^3)	R_{wp} , R_p (%)	χ^2
$(Y_{0.99}Er_{0.01})_2(SO_4)_3$	$Y_{0.99}Er_{0.01})_2(SO_4)_3$	100	<i>Pbcn</i>	a=12.4770 b=9.0354 c=9.8348 V=1108.72(3)	10.68 7.67	3.22
$(Y_{0.99}Er_{0.01})_2(SO_4)_3$ - $(Y_{0.99}Er_{0.01})_2O_2SO_4$ - $(Y_{0.99}Er_{0.01})_2O_2S$ - $(Y_{0.99}Er_{0.01})_2O_3$	$(Y_{0.99}Er_{0.01})_2(SO_4)_3$ $(Y_{0.99}Er_{0.01})_2O_2SO_4$ $(Y_{0.99}Er_{0.01})_2O_2S$ $(Y_{0.99}Er_{0.01})_2O_3$	38.0(0) 26.5(1) 30.6(2) 4.8(8)	<i>Pbcn</i> <i>C2/c</i> <i>P-3m 1</i>	a=12.4804 b=9.0406 c=9.8392 V=1110.16(0) a=14.3439 b=4.2850 c=8.3858 V=493.09(1) a=3.7800 c=6.5631 V=81.21(3) a=10.6051 V=1192.73(6)	6.54 5.11	1.22
$(Y_{0.99}Er_{0.01})_2O_2S$ - $(Y_{0.99}Er_{0.01})_2O_3$	$(Y_{0.99}Er_{0.01})_2O_2S$ $(Y_{0.99}Er_{0.01})_2O_3$	83.8(7) 16.1(3)	<i>P-3m 1</i> <i>Ia-3</i>	a=3.7801 c=6.5638 V=81.22(6) a=10.6055 V=1192.87(1)	7.98 5.59	2.81
$(Y_{0.99}Er_{0.01})_2O_2S$	$(Y_{0.99}Er_{0.01})_2O_2S$	100	<i>P-3m 1</i>	a=3.7800 c=6.5632 V=81.21(4)	5.01 3.31	1.06

1
2 **Synthesis and Optical Properties RE₂O₂S:Ln (RE = La, Y; Ln = Ce, Eu, Dy, Er)**

3
4 E.I. Sal'nikova^{1,2}, Yu.G. Denisenko^{1,3}, A.S. Aleksandrovsky^{4,5}, I.E. Kolesnikov^{6,7}, E. Lähderanta⁷,
5 P.O. Andreev¹, N.O. Azarapin¹, O.V. Andreev¹, S.A. Basova¹, A.V. Matigorov¹

6
7 ¹Department of Inorganic and Physical Chemistry, Tyumen State University, Tyumen 625003, Russia

8 ²Department of General Chemistry, Northern Trans-Ural Agricultural University, Tyumen, 625003, Russia

9 ³Department of General and Special Chemistry, Industrial University of Tyumen, Tyumen 625000, Russia

10 ⁴Laboratory of Coherent Optics, Kirensky Institute of Physics Federal Research Center KSC SB RAS,
11 Krasnoyarsk 660036, Russia

12 ⁵Institute of Nanotechnology, Spectroscopy and Quantum Chemistry, Siberian Federal University,
13 Krasnoyarsk 660041, Russia

14 ⁶Center for Optical and Laser Materials Research, St. Petersburg State University, St. Petersburg 199034,
15 Russia

16 ⁷Department of Physics, Lappeenranta University of Technology LUT, Lappeenranta 53850, Finland

1 **Captions**

2 Fig.1. Experimental, calculated, and difference Rietveld plot of: a,b) $(RE_{0.99}Ln_{0.01})_2(SO_4)_3$; c,d)
3 $(RE_{0.99}Ln_{0.01})_2(SO_4)_3-(RE_{0.99}Ln_{0.01})_2O_2SO_4-(RE_{0.99}Ln_{0.01})_2O_2S-(RE_{0.99}Ln_{0.01})_2O_3$; e,f) $(RE_{0.99}Ln_{0.01})_2O_2S -$
4 $(RE_{0.99}Ln_{0.01})_2O_3$; g,h) $(RE_{0.99}Ln_{0.01})_2O_2S$.

5 Fig. 2. SEM image of a) $(La_{0.99}Dy_{0.01})_2(SO_4)_3$; b) $(La_{0.99}Dy_{0.01})_2O_2S$

6 Fig. 3. Coordination polyhedron structure La_2O_2S

7 Fig. 4. Excitation and emission spectra of $Y_2O_2S:Dy^{3+}$ and $La_2O_2S:Dy^{3+}$ phosphors

8 Fig. 5. Excitation and emission spectra of $Y_2O_2S:Er^{3+}$ and $La_2O_2S:Er^{3+}$ phosphors

9 Fig. 6. Excitation and emission spectra of $Y_2O_2S:Eu^{3+}$ and $La_2O_2S:Eu^{3+}$ phosphors

10 Fig. 7. Excitation and emission spectra of $Y_2O_2S:Ce^{3+}$ and $La_2O_2S:Ce^{3+}$ phosphors

11

12

13

14

15

16

17

18

19

20

21

22

23

24

25

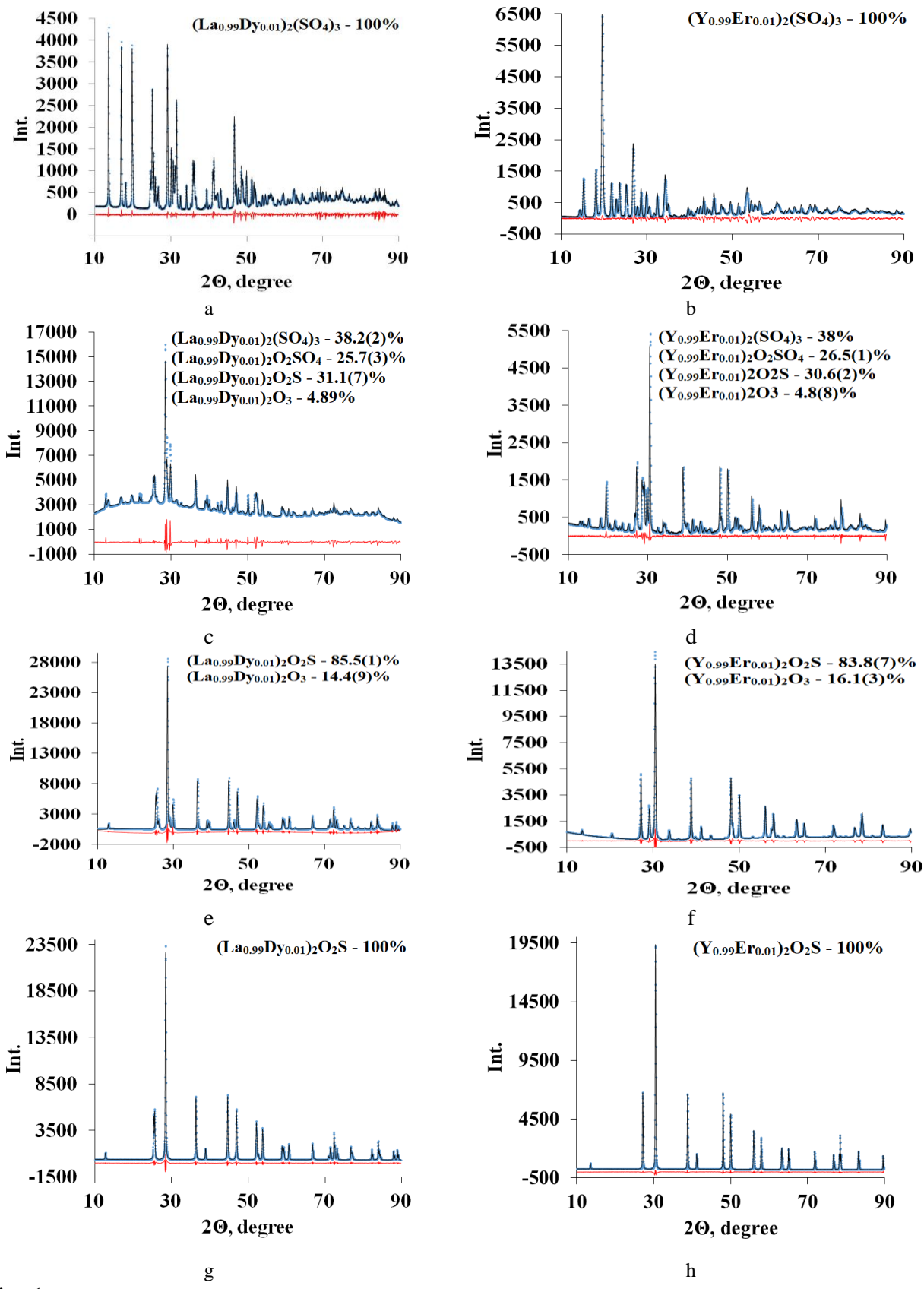
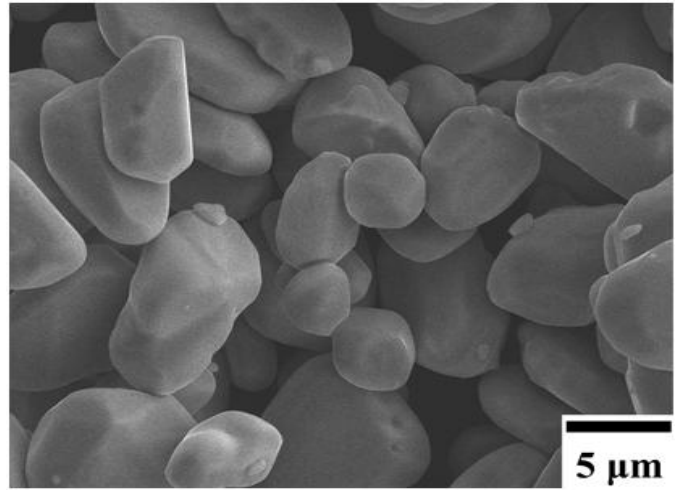
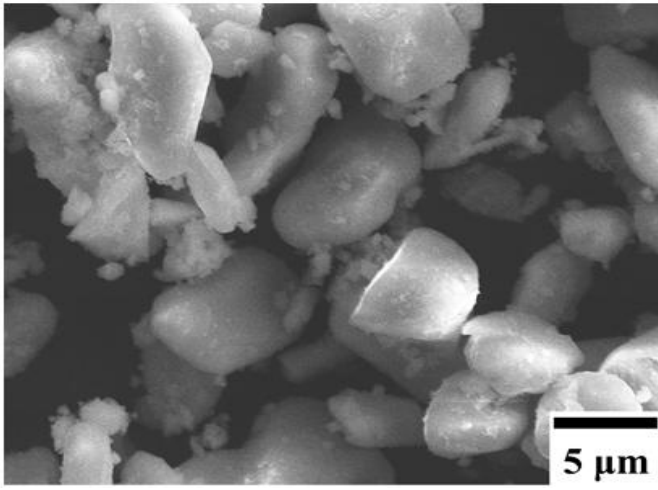


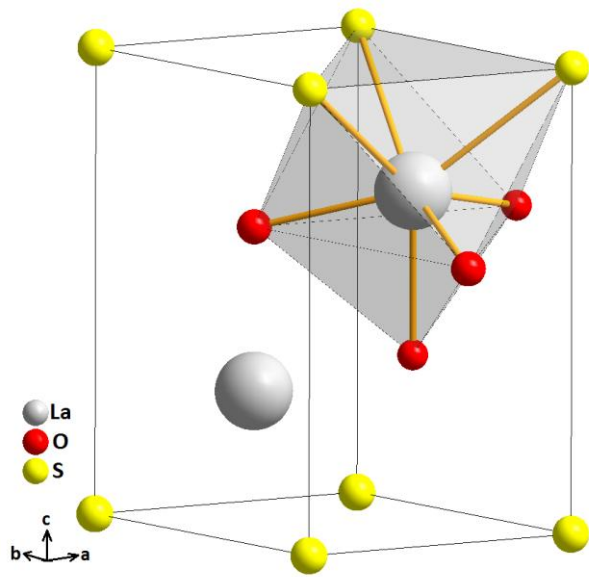
Fig. 1



a)

b)

1 Fig. 2



2
3
4
5
6
7
8
9

Fig. 3.

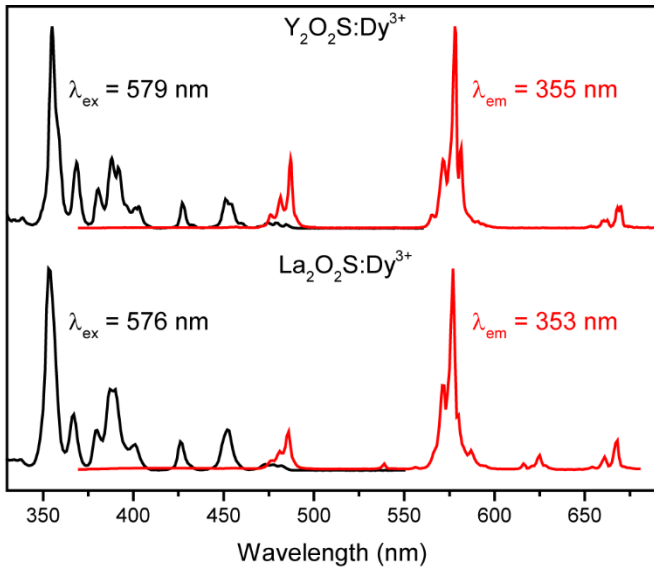


Fig. 4

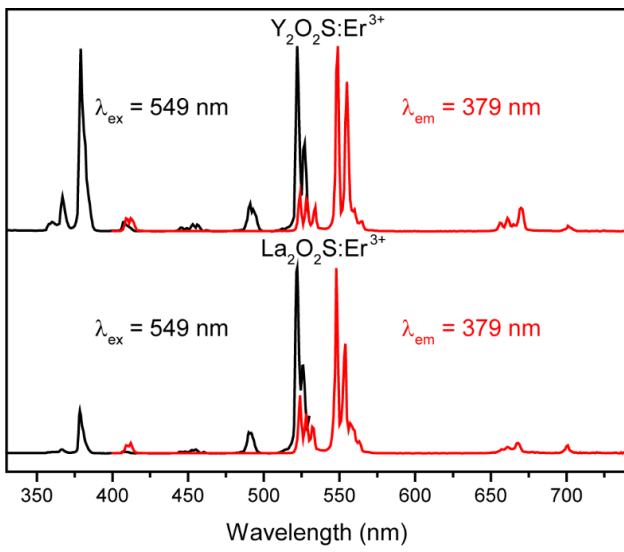


Fig. 5

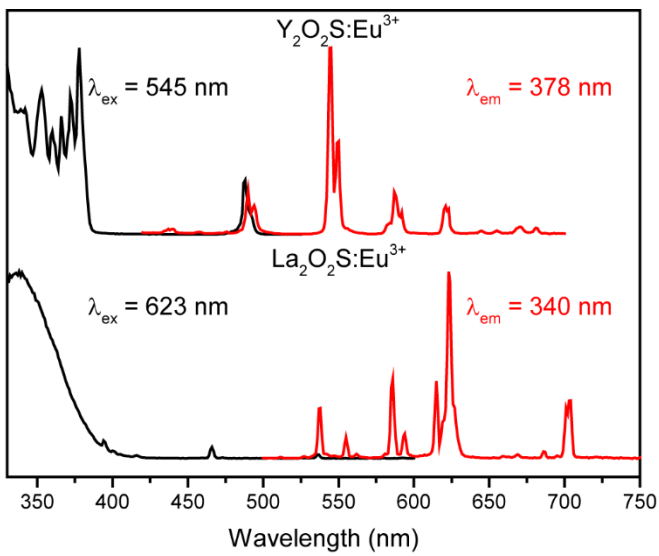
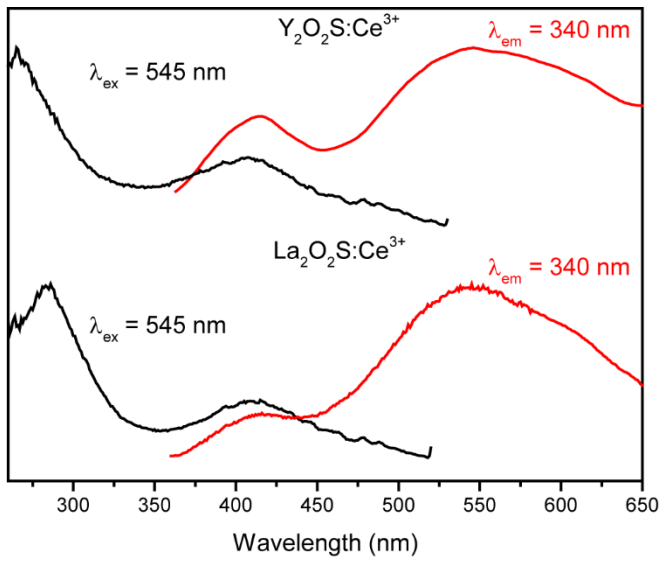


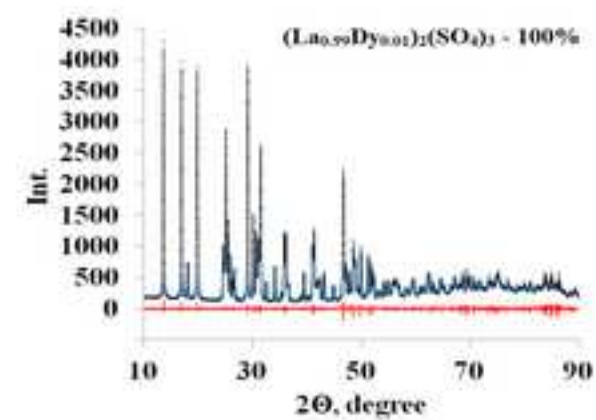
Fig. 6



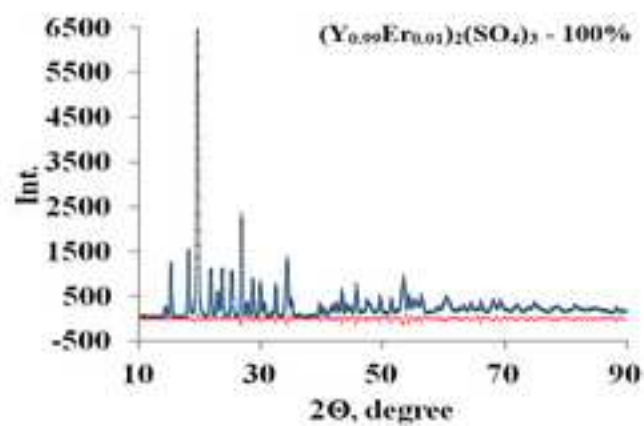
1
2 Fig. 7
3

Figure(s)

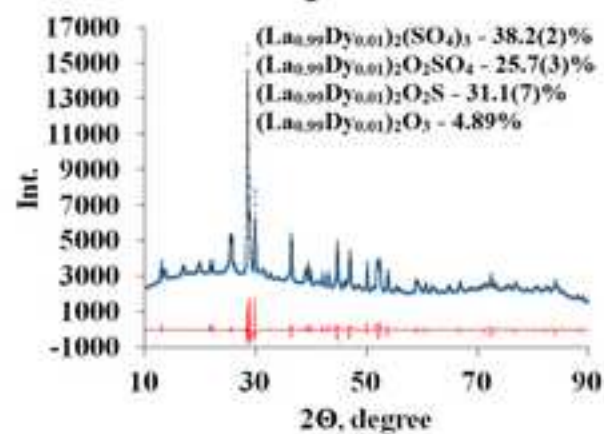
[Click here to download high resolution image](#)



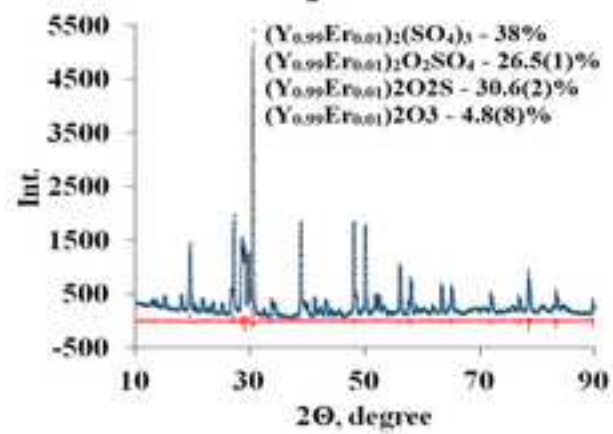
a



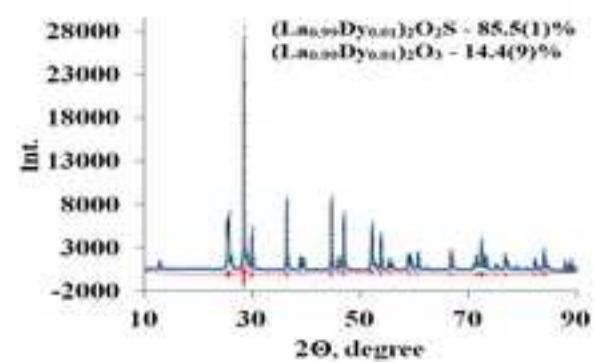
b



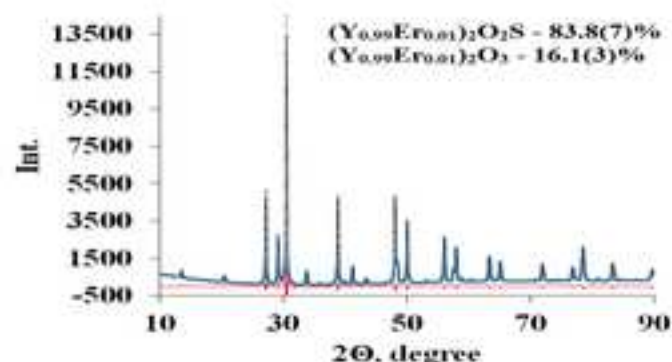
c



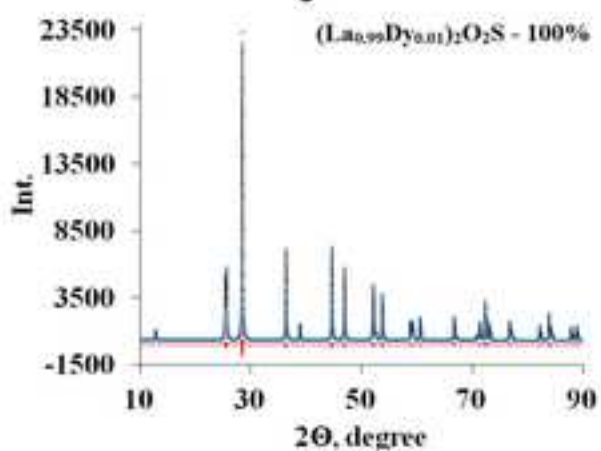
d



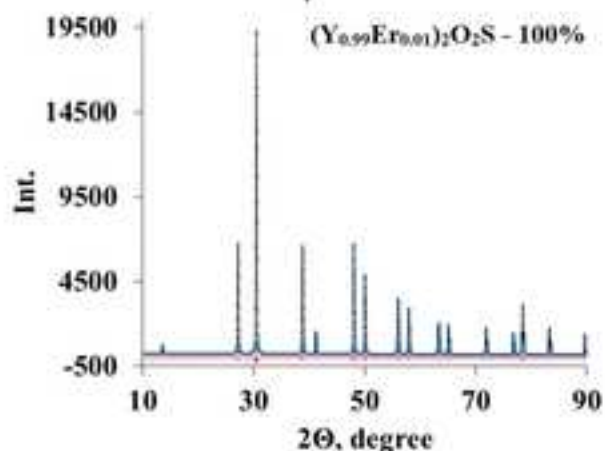
e



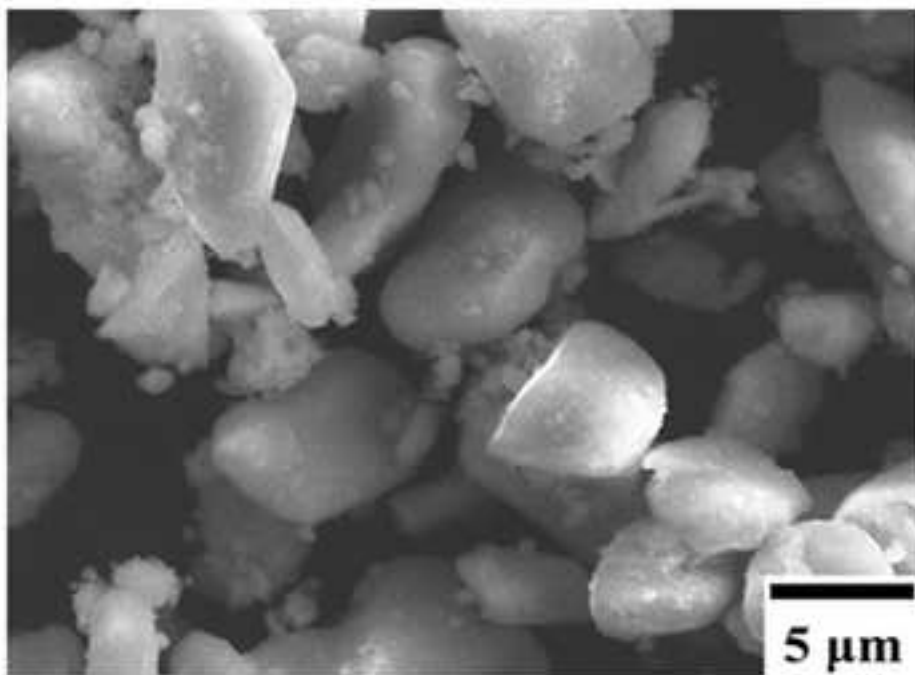
f



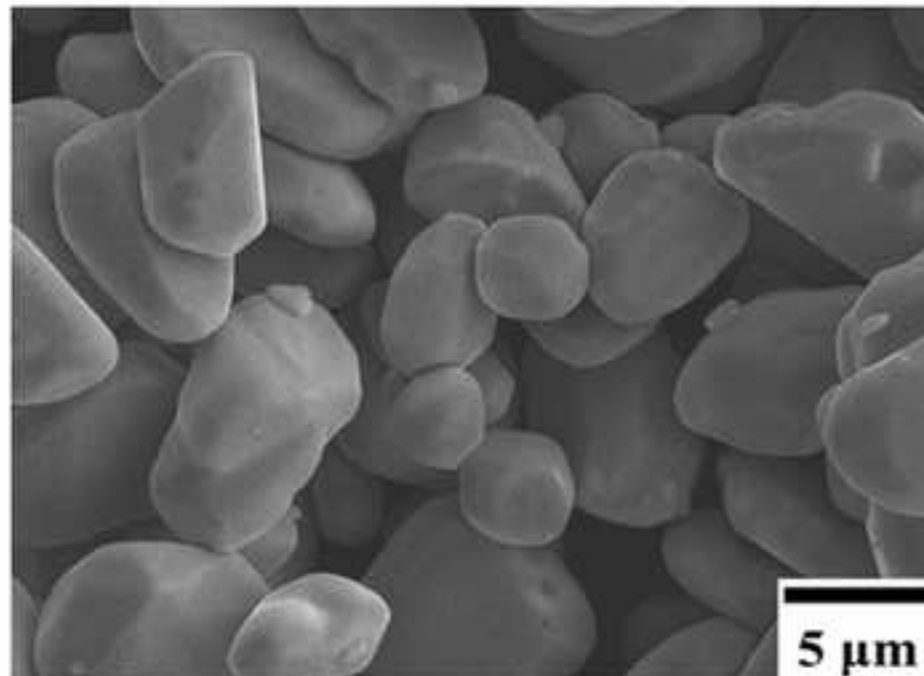
g



h

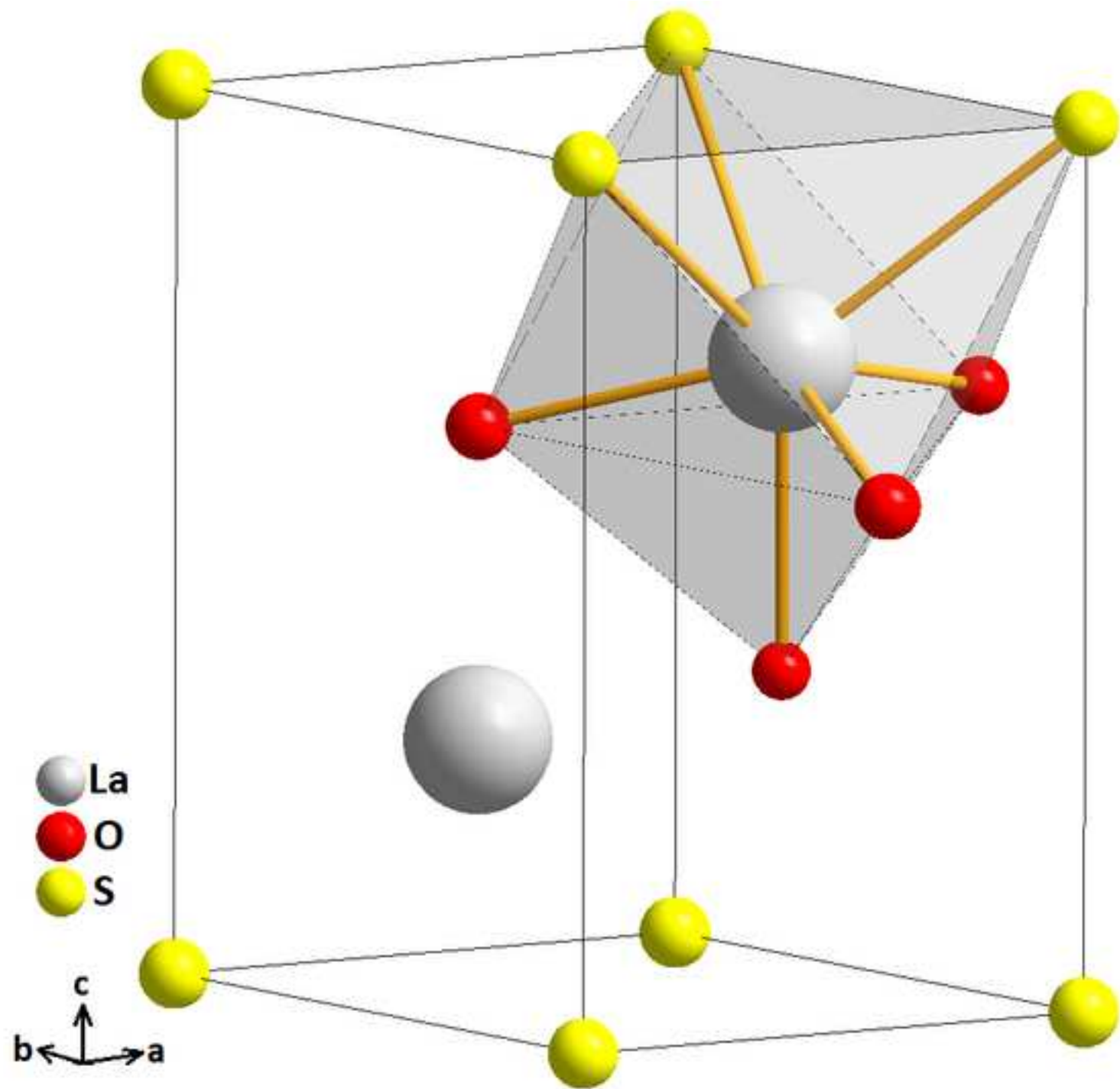


a)



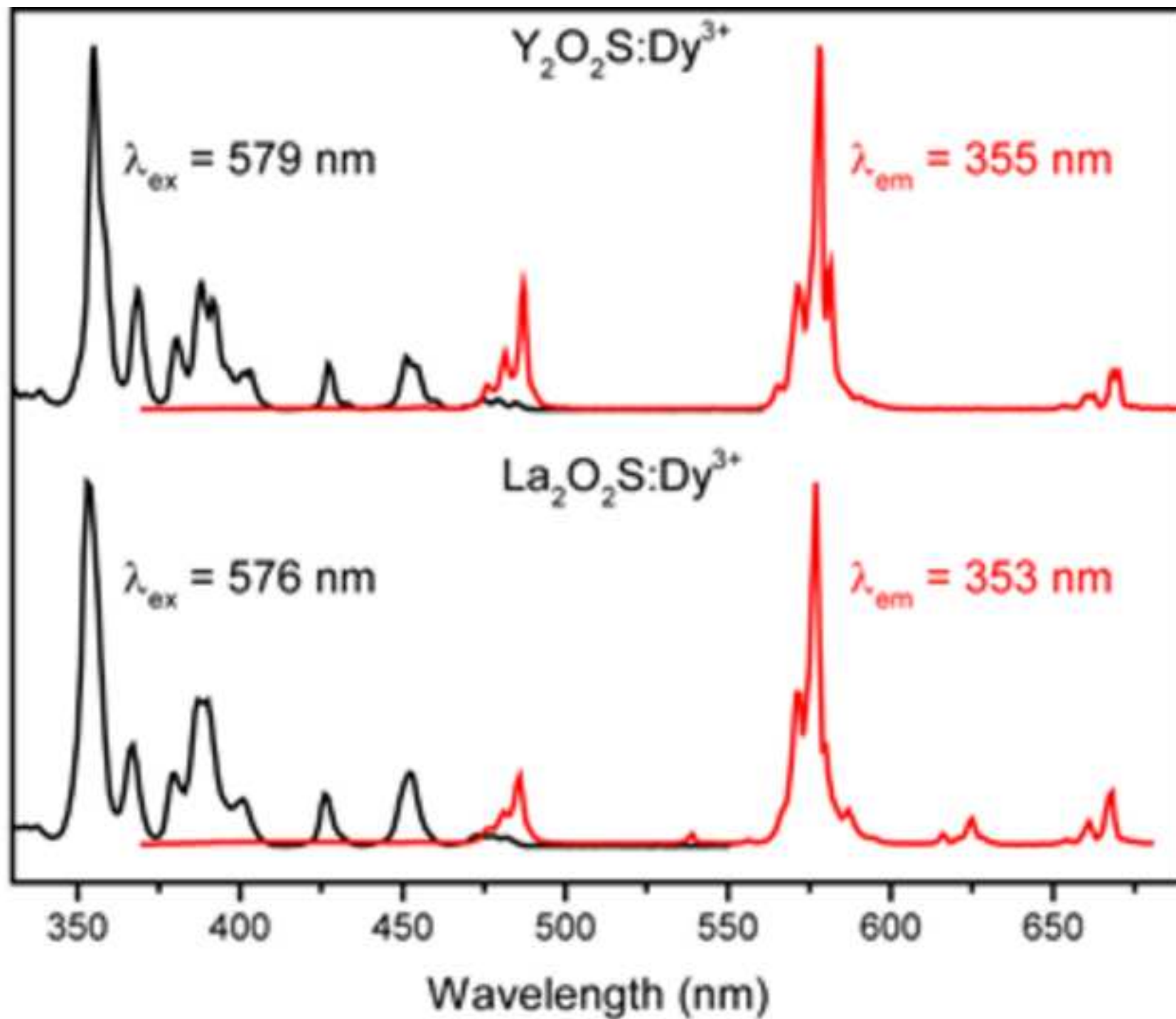
b)

Figure(s)
[Click here to download high resolution image](#)



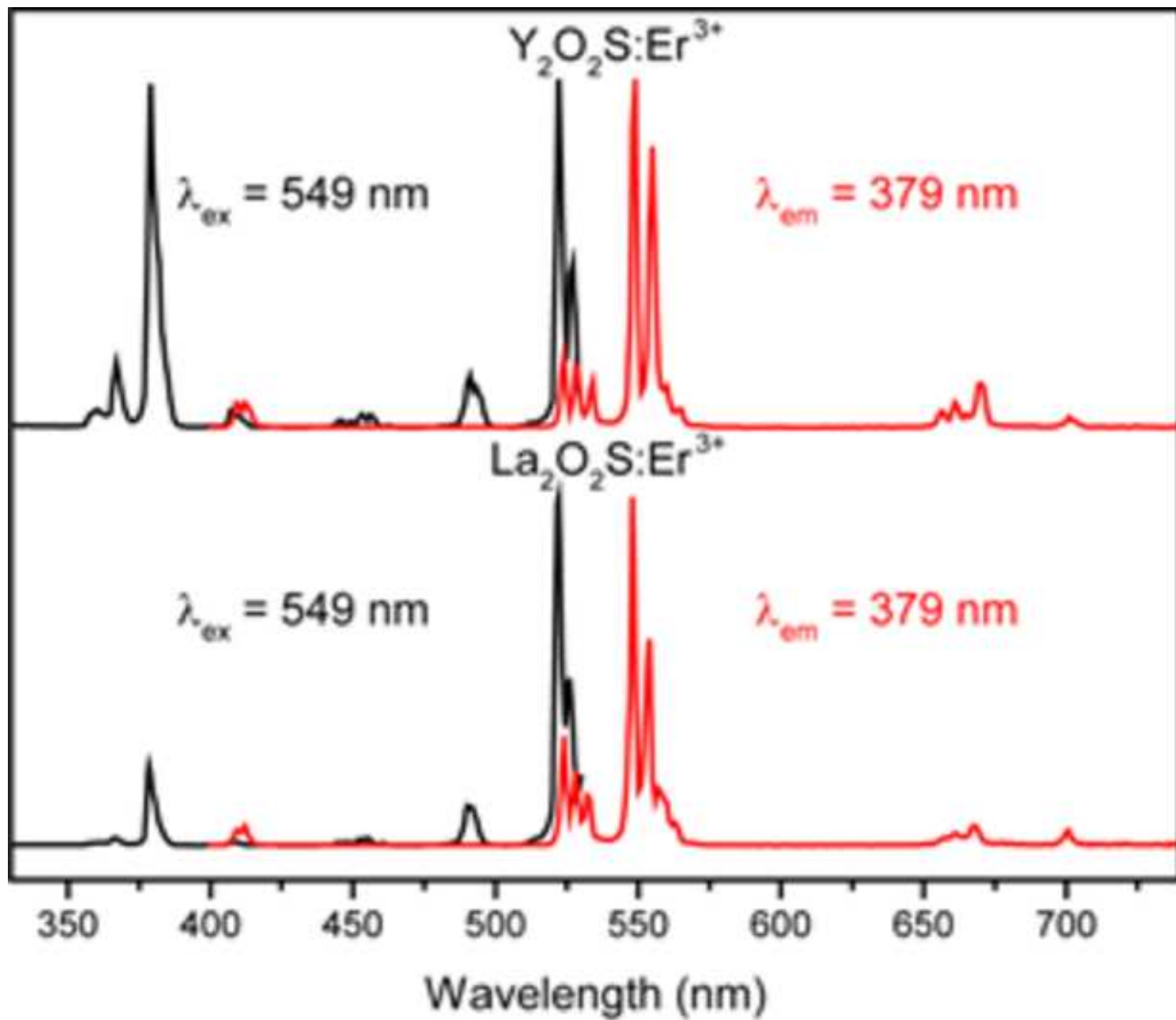
Figure(s)

[Click here to download high resolution image](#)



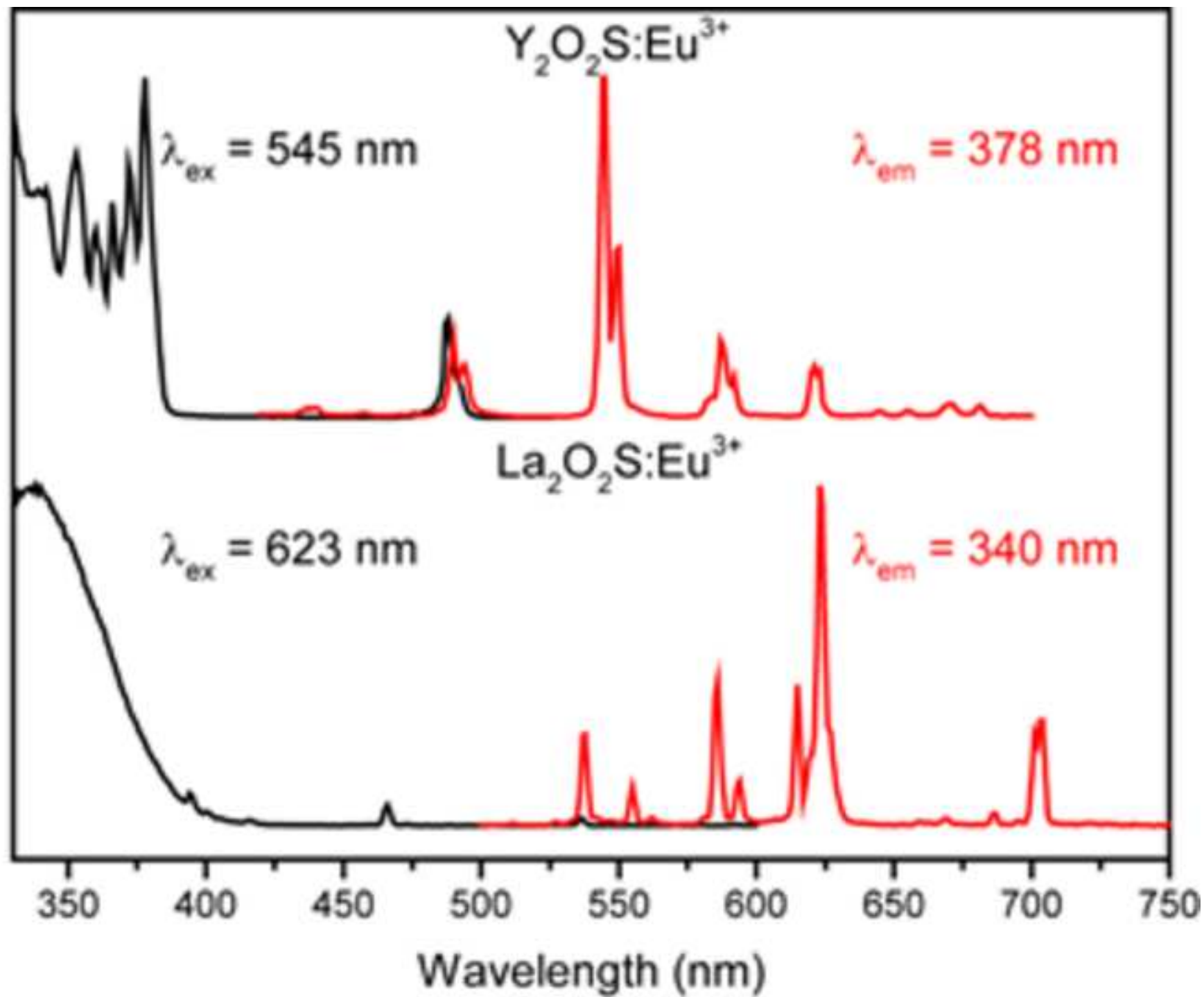
Figure(s)

[Click here to download high resolution image](#)



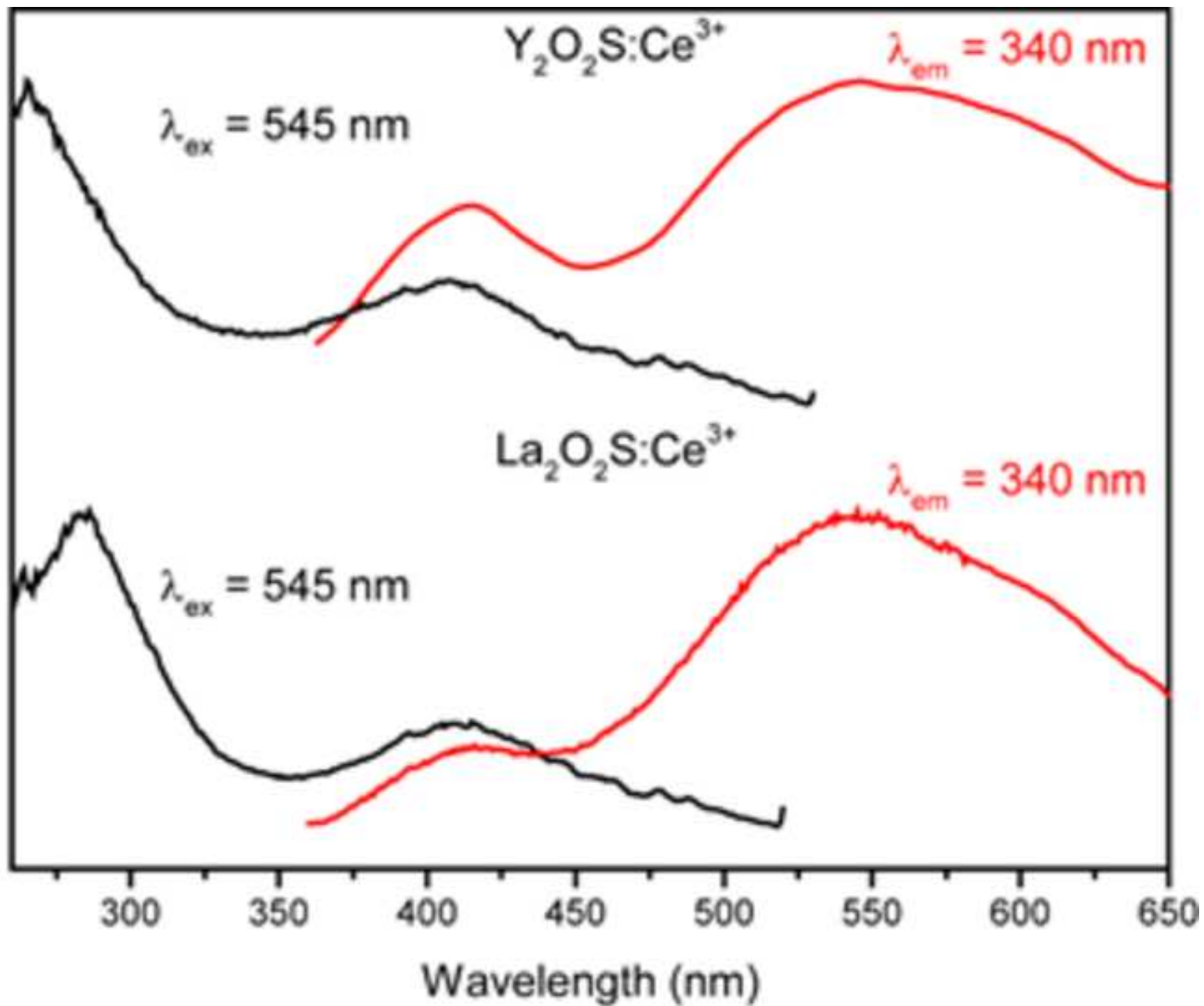
Figure(s)

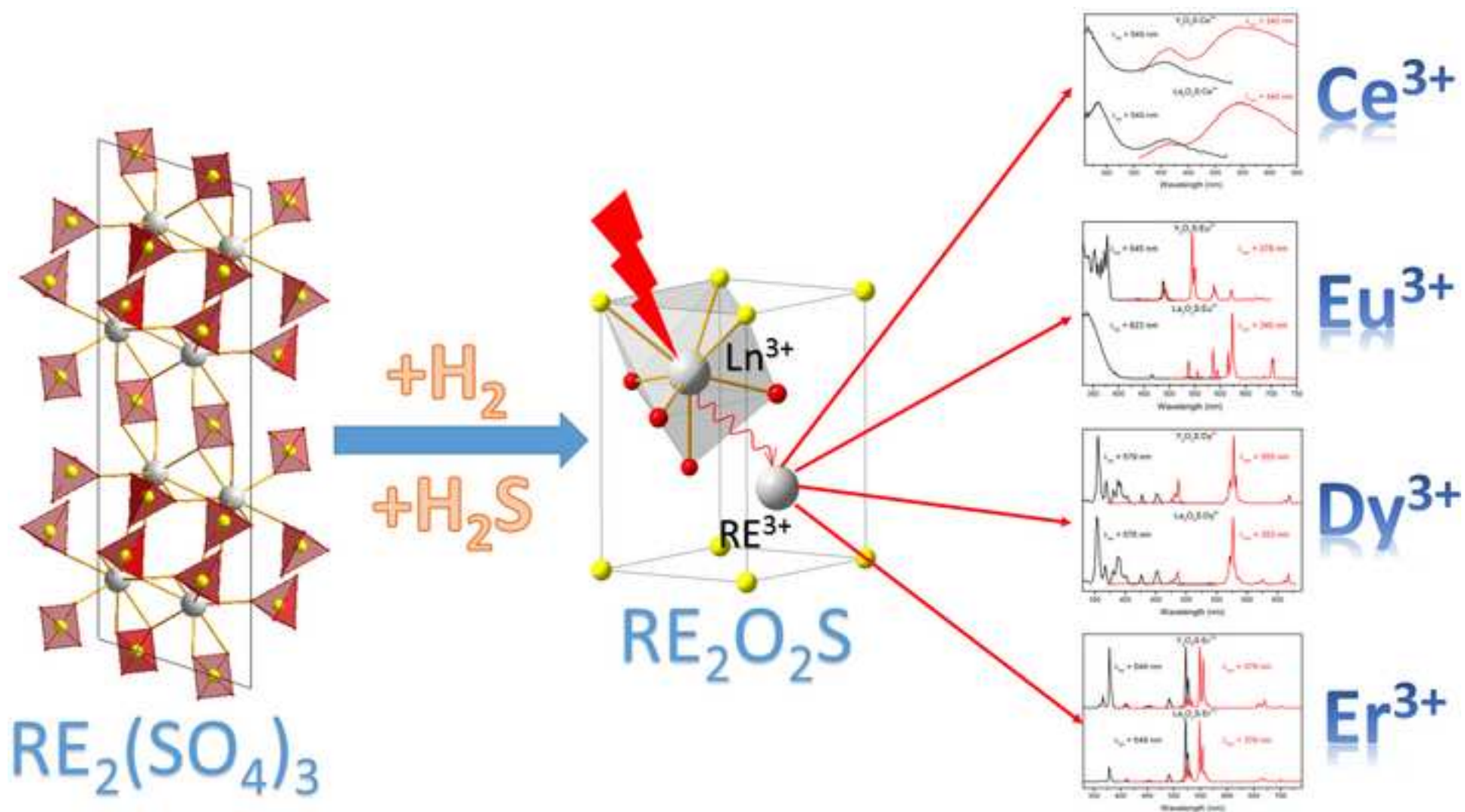
[Click here to download high resolution image](#)

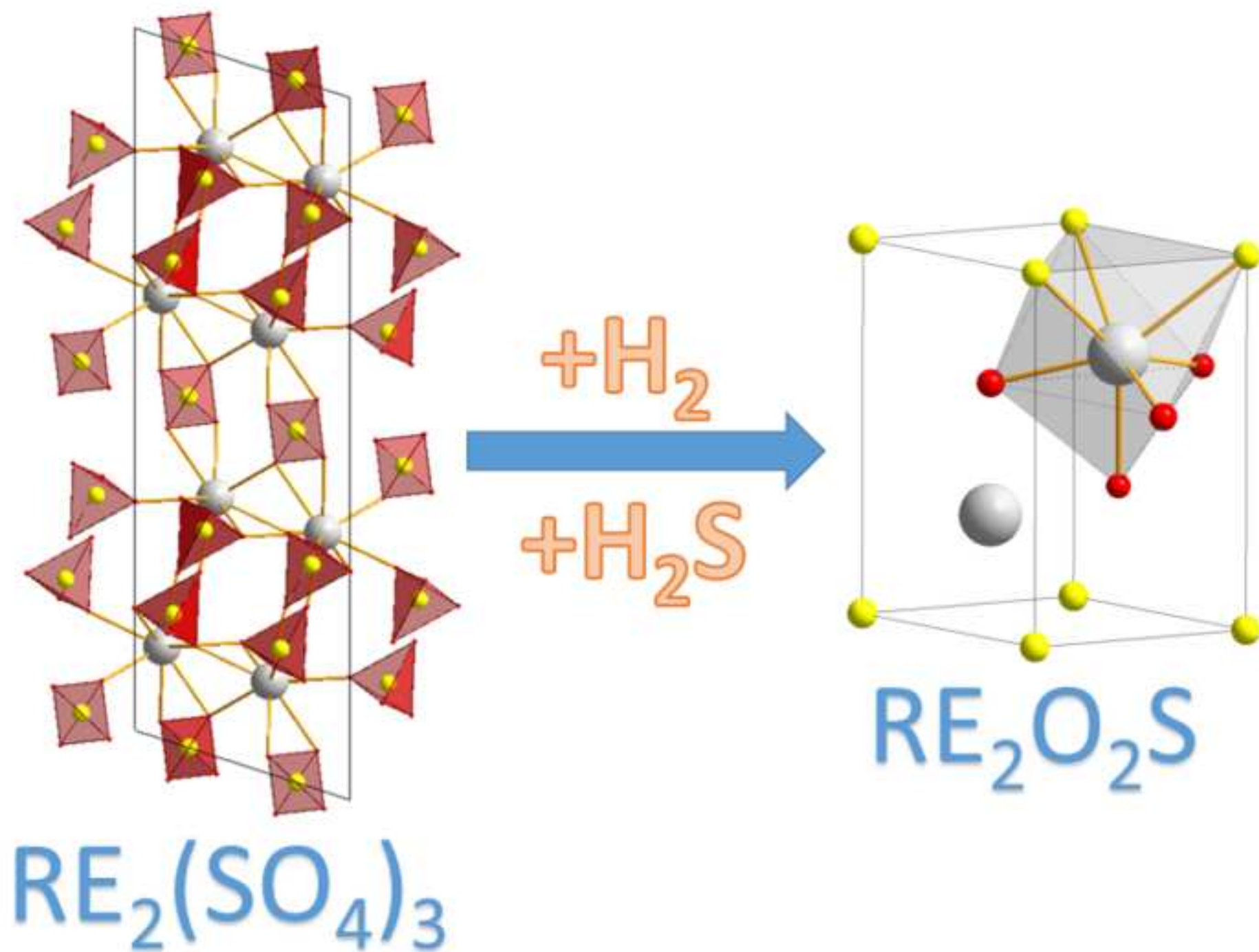


Figure(s)

[Click here to download high resolution image](#)







Supplemental Data

[Click here to download Supplemental Data: Supplementary material.docx](#)